Autoimmunity and immunodeficiency associated with monoallelic LIG4 mutations via haploinsufficiency

Annaïse J. Jauch, MD, PhD, Olivier Bignucolo, PhD, Sayuri Seki, DVM, PhD, Marie Ghraichy, PhD, Ottavia M. Delmonte, MD, Valentin von Niederhäusern, MSc, Rebecca Higgins, PhD, Adhideb Ghosh, PhD, Masako Nishizawa, PhD, Mariko Tanaka, MD, PhD, Adrian Baldrich, MSc, Julius Köppen, MD, Julia R. Hirsiger, MSc, Robin Hupfer, MSc, Stephan Ehl, MD, Anne Rensing-Ehl, MD, Helmut Hopfer, MD, Spasenija Savic Prince, MD, Stephen R. Daley, PhD, Florian A. Marquardsen, PhD, Benedikt J. Meyer, MD, PhD, Michael Tamm, MD, Thomas D. Daikeler, MD, Tamara Diesch, MD, Thomas Kühne, MD, Arthur Helbling, MD, Caroline Berkemeier, MD, PhD, Ingmar Heijnen, PhD, Alexander A. Navarini, MD, PhD, Johannes Trück, MD, PhD, Jean-Pierre de Villartay, PhD, Annette Oxenius, PhD, Christoph T. Berger, MD, Christoph Hess, MD, PhD, Luigi D. Notarangelo, MD, Hiroyuki Yamamoto, MD, PhD, Mike Recher, MD

PII: S0091-6749(23)00422-0

DOI: https://doi.org/10.1016/j.jaci.2023.03.022

Reference: YMAI 15926

To appear in: *Journal of Allergy and Clinical Immunology*

Received Date: 28 March 2022

Revised Date: 24 February 2023

Accepted Date: 6 March 2023

Please cite this article as: Jauch AJ, Bignucolo O, Seki S, Ghraichy M, Delmonte OM, von Niederhäusern V, Higgins R, Ghosh A, Nishizawa M, Tanaka M, Baldrich A, Köppen J, Hirsiger JR, Hupfer R, Ehl S, Rensing-Ehl A, Hopfer H, Prince SS, Daley SR, Marquardsen FA, Meyer BJ, Tamm M, Daikeler TD, Diesch T, Kühne T, Helbling A, Berkemeier C, Heijnen I, Navarini AA, Trück J, de Villartay J-P, Oxenius A, Berger CT, Hess C, Notarangelo LD, Yamamoto H, Recher M, Autoimmunity and immunodeficiency associated with monoallelic LIG4 mutations via haploinsufficiency, *Journal of Allergy and Clinical Immunology* (2023), doi: https://doi.org/10.1016/j.jaci.2023.03.022.

Title:
Autoimmunity and immunodeficiency associated with monoallelic *LIG4* mutations *via* haploinsufficiency

Annaïse J. Jauch, MD, PhD[1] • Olivier Bignucolo, PhD[2] • Sayuri Seki, DVM, PhD[3] • Marie Ghraichy, PhD[4] • Ottavia M. Delmonte, MD[5] • Valentin von Niederhäusern, MSc[4] • Rebecca Higgins, PhD[6] • Adhideb Ghosh, PhD[6,7] • Masako Nishizawa, PhD[3] • Mariko Tanaka, MD, PhD[8] • Adrian Baldrich, MSc[1] • Julius Köppen, MD[1] • Julia R. Hirsiger, MSc[9] • Robin Hupfer, MSc[1] • Stephan Ehl, MD[10] • Anne Rensing-Ehl, MD[10] • Helmut Hopfer, MD[11] • Spasenija Savic Prince, MD[11] • Stephen R. Daley, PhD[12] • Florian A. Marquardsen, PhD[1] • Benedikt J. Meyer, MD, PhD[1] • Michael Tamm, MD[13] • Thomas D. Daikeler, MD[14,22] • Tamara Diesch, MD[15] • Thomas Kühne, MD[15] • Arthur Helbling, MD[16] • Caroline Berkemeier, MD, PhD[17] • Ingmar Heijnen, PhD[17] • Alexander A. Navarini, MD, PhD[6,22] • Johannes Trück, MD, PhD[4] • Jean-Pierre de Villartay, PhD[18] • Annette Oxenius, PhD[19] • Christoph T. Berger, MD [9,22] • Christoph Hess, MD, PhD[20,21,22] • Luigi D. Notarangelo, MD[5], Hiroyuki Yamamoto, MD, PhD[1,3,*] and Mike Recher[1,22,*] MD

[1]Immunodeficiency Laboratory, Department of Biomedicine, University of Basel and University Hospital of Basel, Switzerland.
[2]Swiss Institute of Bioinformatics, Basel, Switzerland
[3]AIDS Research Center, National Institute of Infectious Diseases, Tokyo, Japan
[4]Division of Immunology and Children's Research Center, University Children's Hospital Zurich, University of Zurich (UZH), Switzerland
[5]Laboratory of Clinical Immunology and Microbiology, National Institute of Allergy and Infectious Diseases, National Institutes of Health, Bethesda, MD, USA.
[6]Division of Dermatology and Dermatology Laboratory, Department of Biomedicine, University and University Hospital of Basel, Basel, Switzerland.
[7]Competence Center for Personalized Medicine, University of Zürich/Eidgenössische Technische Hochschule (ETH), Zürich, Switzerland.
[8]Department of Pathology, The University of Tokyo, Tokyo, Japan
[9]Translational Immunology, Department of Biomedicine, University of Basel, Basel, Switzerland
[10]Institute for Immunodeficiency, Center for Chronic Immunodeficiency, Medical Center, Faculty for Medicine, University of Freiburg, Germany.
[11]Institute for Pathology, University Hospital Basel, Basel, Switzerland.
[12]Centre for Immunology and Infection Control, School of Biomedical Sciences, Faculty of Health, Queensland University of Technology, Brisbane 4000, Queensland, Australia.
[13]Department of Pneumology, University Hospital Basel, Switzerland
[14]Department of Rheumatology, University Hospital Basel, Switzerland
[15]Division of Pediatric Oncology/Hematology, University Children's Hospital Basel, Switzerland
[16]Division of Allergology and clinical Immunology, Department of Pneumology and Allergology, Inselspital, Bern University Hospital, University of Bern, Bern, Switzerland
[17]Division Medical Immunology, Laboratory Medicine, Hospital Basel, Basel University, Switzerland
[18]Laboratory of Genome Dynamics in the Immune System, INSERM UMR1163, Université Paris Descartes Sorbonne Paris Cité, Institut Imagine, Paris, France.
[19]Institute of Microbiology, Eidgenössische Technische Hochschule (ETH), Zürich, Switzerland.
[20]Immunobiology Laboratory, Department of Biomedicine, University and University Hospital of Basel, Basel, Switzerland.
[21]Cambridge Institute of Therapeutic Immunology & Infectious Disease, Department of Medicine, University of Cambridge, Cambridge, UK.
[22]University Center for Immunology, University Hospital Basel, Switzerland

*Hiroyuki Yamamoto and Mike Recher are shared senior authors

Correspondence:
1) Mike Recher, University Immunology Center, University Hospital, Basel, Switzerland and Immunodeficiency Laboratory, Department Biomedicine, University of Basel, Switzerland; e-mail: mike.recher@usb.ch
2) Hiroyuki Yamamoto, AIDS Research Center, National Institute of Infectious Diseases, Tokyo, Japan; e-mail: h-yamato@niid.go.jp

Funding
MR was supported by the Swiss National Science Foundation (PP00P3_181038 and 310030_192652). AJ was supported by the Swiss Cancer League (SNF 323630_151483) and Novartis Foundation for Medical-Biological Research. This work was supported by grants from the Swiss National Supercomputing Center (CSCS) for OB under the project IDs sm09 and s1099. JT was supported by the Swiss National Science Foundation (PZ00P3_161147 and PZ00P3_1837777). SE was supported by the BMBF GAIN consortium (TP6; 01GM1910A). This work was partially supported by the Japan Agency for Medical Research and Development (AMED) (Grant numbers JP19fm0208017 and JP22wm0325006) and the Takeda Science Foundation for HY. HY was supported by the Swiss National Science Foundation (310030_192652). SS was supported by the Ministry of Education, Culture, Sports, Science and Technology (MEXT) in Japan (JSPS) Grant-in-Aid for Early-Career

Scientists [22K15480]. LDN is supported by the Division of Intramural Research, National Institute of Allergy and Infectious Diseases, National Institutes of Health, Bethesda, MD, USA

Conflict of Interest Disclosure

The authors declare no competing financial interests.

Abstract

Background: Biallelic mutations in *LIG4* encoding DNA-ligase 4 cause a rare immunodeficiency syndrome manifesting as infant-onset life-threatening and/or opportunistic infections, skeletal malformations, radiosensitivity and neoplasia. LIG4 is pivotal during DNA repair and during V(D)J recombination as it performs the final DNA-break sealing step.

Objective: We explored whether monoallelic *LIG4* missense mutations may underlie immunodeficiency and autoimmunity with autosomal dominant inheritance.

Methods: Extensive flow-cytometric immune-phenotyping was performed. Rare variants of immune system genes were analyzed by whole exome sequencing. DNA repair functionality and T cell-intrinsic DNA damage tolerance was tested with an ensemble of *in vitro* and *in silico* tools. Antigen-receptor diversity and autoimmune features were characterized by high-throughput sequencing and autoantibody arrays. Reconstitution of wild-type *vs.* mutant *LIG4* were performed in *LIG4* knock-out Jurkat T cells and DNA damage tolerance was subsequently assessed.

Results: A novel heterozygous LIG4 loss-of-function mutation (p.R580Q), associated with a dominantly inherited familial immune-dysregulation consisting of autoimmune cytopenias, and in the index patient with lymphoproliferation, agammaglobulinemia and adaptive immune cell infiltration into nonlymphoid organs. Immunophenotyping revealed reduced naïve $CD4^+$ T cells and low TCR-V$\alpha$$7.2^+$ T cells, while T/B-cell receptor repertoires showed only mild alterations. Cohort screening identified two other non-related patients with the monoallelic *LIG4* mutation p.A842D recapitulating clinical and immune-phenotypic dysregulations observed in the index family and displaying T cell-intrinsic DNA damage intolerance. Reconstitution experiments and molecular dynamics simulations categorize both missense mutations as loss-of-function and haploinsufficient.

Conclusion: We provide evidence that certain monoallelic *LIG4* mutations may cause human immune dysregulation *via* haploinsufficiency.

Clinical implications

LIG4 haploinsufficiency should be considered in patients with immune dysregulation of unidentified cause, as it may have prognostic as well as therapeutic consequences.

Capsule Summary

This is the first description of LIG4 haploinsufficiency-associated combined immunodeficiency in humans.

Key words

DNA ligase 4 – DNA damage - autoimmunity – haploinsufficiency – autosomal dominant – inborn errors of immunity – immunodeficiency – primary immunodeficiency

Abbreviations

AIHA (autoimmune hemolytic anemia), AIRR-seq (adaptive immune receptor repertoire-sequencing), autoinflamm. (autoinflammation), BCR (B cell receptor), BE (Binding energy), cDNA (copy deoxyribonucleic acid), CDR3 (complementarity-determining region 3), CID (combined immunodeficiency), comp. het. (compound heterozygous), CTV (CellTrace™ violet), DSB (DNA double-strand breaks), HD (healthy donors), homo. (homozygous), IGH (immunoglobulin heavy chain), IGHA (immunoglobulin heavy constant alpha), IGHG (immunoglobulin heavy constant gamma), IgL (immunoglobulin light constant), IR (ionizing radiation), ITP (immune thrombocytopenia), LAG3 (lymphocyte-activation gene-3), LIG4 (DNA ligase 4), MD (molecular dynamics), mRNA (messenger ribonucleic acid), NHEJ (nonhomologous end-joining), OBD (Oligonucleotide/ oligosaccharide-fold domain), OH (hydroxyl), PBMC (peripheral blood mononucleated cells), PAD (primary antibody deficiency), PCR (polymerase chain reaction), PD-1 (programmed cell death-1), PID (primary

immunodeficiency), SCID (severe combined immunodeficiency), SHM (somatic hypermutations), TCR (T cell receptor), TCRA (T cell receptor α-chain), TCRB (T cell receptor β-chain), WES (whole exome-sequencing), WT (wild-type).

Introduction

The three mammalian DNA ligases (LIG1, LIG3, LIG4) are pivotal for genomic recombination, replication and repair[1]. LIG4 is essential for resolving DNA double-strand breaks (DSB) - the most noxious DNA lesions[2]. DSB mending engages the ubiquitous non-homologous end-joining (NHEJ) repair pathway, which utilizes LIG4 for the last step of DNA re-ligation[2].

NHEJ is preferentially used after genotoxic assaults like ionizing radiation (IR) as well as physiologically during V(D)J recombination, a crucial step in the T and B cell receptor generation (TCR respectively BCR)[3]. V(D)J recombination is mandatory for the development of adaptive immunity, as the variability and consequently, the antigen recognition is ensured by the semi-stochastic recombination of the variable (*V),* diversity (*D*) and joining (*J*) gene segments encoding the variable domains of both T and B cell receptors[3]. A well-regulated DNA-damage response is therefore imperative for immune homeostasis and to guarantee immunocompetence and immune tolerance.

Although the first LIG4 deficient patient was characterized 33 years ago, only 120 patients with either homozygous or compound heterozygous mutated *LIG4* have been published to date **(**reviewed in **Table I)**. LIG4 haploinsufficiency caused by monoallelic *LIG4* mutations has not been reported in human patients, whereas murine data suggests that a single functional *LIG4* allele may not be sufficient to protect from malignancy and may reduce survival[4-6]. Here we identified two novel monoallelic *LIG4* missense variants associated with impaired tolerance to DNA damage in primary T cells and combined immunodeficiency, in four patients from three non-related families.

Methods

Ethics approval and human subjects

Following informed consent, the patients and family members were included into a prospective cohort that was approved by the Ethics committee of the Northwestern and central Switzerland (EKNZ 2015-187), complying with all national and international ethical regulations. Blood samples from healthy donors were obtained after informed consent from the Blood Donor Center, University Hospital Basel.

Genetic analysis

Genomic DNA was isolated from cultured T-cell blasts or peripheral blood mononuclear cells (PBMCs) using the QIAamp DNA Blood Mini Kit (Qiagen). Whole exome sequencing was performed as described earlier[7, 8].

The *LIG4* variant was confirmed by Sanger sequencing of PCR amplification products of cDNA derived from PBMCs. After running the amplicon on an 1.5% agarose gel, DNA was extracted with QIAquick Gel Extraction Kit (Qiagen). The purified PCR products were then bidirectionally sequenced by Microsynth (Switzerland).

Cell isolation and immunophenotyping

Patient- and healthy control-derived PBMCs were isolated from whole blood, *via* Ficoll density gradient separation using Lymphoprep™ (density 1.077g/mL, Axonlab).

Cells were stained in PBS containing 2.5% human AB serum, NaH_3 0.01%, Hepes 25mM, Fc block (BioLegend # 426101) for 30min at 4°C. Chemokine receptor staining was performed at 37°C for 20min. All primary/ secondary antibody conjugates are listed in supplemental methods. Cell viability was assessed using Live/Dead

Fixable NIR (# L34975, Invitrogen™, ThermoFisher Scientific). Data analysis was performed using FlowJo software (Version 10.5.2, TreeStar, USA).

Additional methods are reported in the **supplementary material** section.

Results

Dominantly inherited immune-dysregulation

P1, presented at the age of two years with autoimmune hemolytic anemia (AIHA) and immune thrombocytopenia (ITP) **(Fig 1, *A*)**. During the disease course, P1 developed lymphoproliferation (splenomegaly and lymphadenopathy) and multiple infections including opportunistic pathogens **(Fig 1, *A*)**. At the age of eleven years, P1 developed biopsy-proven interstitial nephritis with polyclonal T and B cell infiltrations **(Fig 1, *B*)**. At the transition into the adult immunology service, being under immune suppression with mycophenolate, agammaglobulinemia was noted. Immunoglobulin replacement therapy was started at this time. Despite normalized serum IgG levels, P1 developed life-threatening non-infectious pneumonitis, again characterized by polyclonal lymphocyte infiltration **(Fig 1, *C* - *E*)**. Lastly, sterile granulomatous parotitis was diagnosed **(Fig 1, *F*)**. Her father and two paternal uncles experienced several adult-onset ITP episodes that responded to systemic steroids.

A detailed immunological evaluation was performed in P1 and her father (P2). The father had mildly reduced lymphocytes (1.02 $x10^9$/L) and thrombocytes (114 $x10^9$/L), in the absence of immune modulating treatment **(Table EI)**. Analysis of PBMCs revealed a reduced frequency of naïve $CD27^+CD45RO^-$ T cells in both patients **(Fig 1, *G* and *H*)**. T cell proliferation upon mitogen stimulation was enhanced **(Fig 1, *I*)**. Peripheral blood-derived $CD4^+$ T regulatory cells (T_{reg}, $CD25^{hi}CD127^{low}$) were reduced in frequency in both P1 and her father compared to healthy donors (HDs) **(Fig E1, *A*)**. Those T_{reg} displayed an activated and proinflammatory phenotype **(Fig E1, *B*)**. $CD4^+$ T cells also displayed a phenotype skewed towards T_{H1} **(Fig E1, *C*)**. Autoreactivity of B cells was investigated by probing the father's serum immunoglobulins against different self-antigens on a protein microarray and compared with gender-matched controls. Four of the tested IgG autoantibody specificities were found to be elevated in the serum of the father **(Fig E1, *D* and *F*)**, including augmented IgG directed against genomic DNA **(Fig E1, *E*)**. Endogenous IgG of P1 could not be tested due to the agammaglobulinemia and the immunoglobulin substitution. Low T cells bearing the TCR $V\alpha7.2^+$ were noted in both **(Fig 1, *J*)**, similarly to what was found in some other patients diagnosed with CID in our cohort **(Fig 1, *K*)**.

Since low TCR $V\alpha7.2^+$ T cells have been reported as a hallmark observed in patients with V(D)J recombination defects[9, 10], we performed TCR and BCR high throughput sequencing.

Preserved TCR/BCR repertoires

The most common TCR loci were sequenced, using DNA derived from peripheral blood T cells from P1 and her parents. The distribution of the most variable region of the TCR, the complementarity-determining region 3 (CDR3) lengths in the T cell receptor α-chain (*TCRA,* **Fig 2, *A***) and β-chain (*TCRB*) sequences **(Fig E2, *A*)** were comparable in P1 and her parents. To account for the entire repertoire diversity and clonality, the Shannon's (*H)* entropy[11] and Simpson's clonality[12] indices were computed and found to be normal **(Fig 2, *B* and *C,* respectively)**.

We focused on the individual *TCRA V* gene segment usage, as this locus can adopt a directional multistage recombination, which is halted only upon positive thymocyte selection[13]. We found only the V-gene segment *27-01-03* to be significantly overrepresented in the two patients compared to healthy donors (HD) (**Fig 2, *D***).

To investigate the pairing of *TCRA V* with *J* gene segments, heatmaps were computed. The pairing was overall maintained, in total **(Fig E2, *B*)** as well as in unique *TCRA* sequences (**Fig 2, *E***), including distal gene segment pairing **(Fig 2, *E*, Fig E2, *B*)**.

The autoimmune disposition in P1 and her father could reflect differences in B cell subsets and/or BCR repertoire, thus peripheral blood B cells were immunophenotyped and RNA-derived immunoglobulin heavy chain (*IGH*) repertoires were sequenced using isotype-resolved barcode based adaptive immune receptor repertoire-sequencing (AIRR-seq) technology.

P1 displayed an inverted BCR light chain (κ *vs.* λ) expression on B cells compared to HDs **(Fig 2, *F*)**. Both patients had an increased percentage of $CD21^{low}$ B cells **(Table EI)**. The vast majority of P1's B cells included unmutated naïve and memory IgM/IgD (*MD*) transcripts **(Fig E2, *C*)**. Further, the constant region segment utilization was investigated **(Fig 2, *G*)**. In P1 IgG (*IGHG*) and IgA (*IGHA*) transcripts were barely detectable **(Fig E2, *C*)**. Both patients displayed a tendency for a reduced *IGHG2* subclass frequency **(Fig 2, *H*)**. In addition, P1's B cells transcripts showed a skewing towards the utilization of the *IGHG3* subclass **(Fig 2, *H*)**.

P1's *MD* memory B cells had an increased usage of the V_H4 gene family at the expense of V_H3 **(Fig 2, *I*)**. In both patients the memory *MD* B cell transcripts harbored less abundantly the J_H4 gene segment **(Fig 2, *J*).**

Affinity maturation was analyzed *via* the quantification of somatic hypermutations (SHM) detected in memory B cell transcripts, being below the normal range for P1 and marginally low in the paternal memory *MD* compartment **(Fig 2, *K*)**. An increased ratio of replacement mutations (R) compared to silent mutations (S) (R/S ratio) in the CDRs may point at antigen selection[14, 15]. P1's *IGHG* and memory *MD* B cell transcripts showed a decreased R/S ratio compared to HDs **(Fig 2, *L*)**, while in the father's B cells, the R/S ratio was only marginally low in *MD* memory B cells **(Fig 2, *L*)**.

Novel heterozygous *LIG4* missense variant

We next investigated PBMC-derived DNA of P1, her parents and the clinically healthy brother using whole-exome sequencing (WES), followed by custom-designed PID gene panel filtering. In both diseased individuals we detected a c.G1739A heterozygous missense variant in *LIG4* **(Table EII)**. Sanger sequencing confirmed heterozygosity. The healthy mother and brother did both not carry the *LIG4* variant **(Fig 3, *A*)**. The c.G1739A variant causes replacement of an arginine at position 580 by a glutamine (p.R580Q). The Arg580 is highly conserved across various vertebrates **(Fig 3, *B*)** and locates within the oligonucleotide/oligosaccharide-binding domain (OBD), crucial for complete LIG4 encirclement of the DNA during NHEJ[16] **(Fig 3, *C*)**. The variant is predicted to have functional impact on the LIG4 protein (CADD-PHRED score 33[17], PolyPhen-2[18] score 1 and SIFT[19] 21 score 0) **(Table EII)**. This *LIG4* variant has so far not been described in the literature **(Table I).** *LIG4* mRNA was somewhat low in the father when compared to HDs but was normal in P1 **(Fig 3, *D*)**. Immunoblots from T cell blast derived protein revealed conserved LIG4 protein levels in P1 **(Fig 3, *E*)**.

In addition, a novel homozygous missense variant in *FAS* (c.G383A, p.R128K, **Table EII**) was detected in the father. Both children, P1 and her healthy brother, were heterozygous carriers for this *FAS* variant. Based on unobtrusive FAS-related serum biomarkers, normal FAS-related apoptosis studies in T cell blasts of P1 and the fact that the healthy brother carried the same heterozygous *FAS* variant, we excluded the rare *FAS* variant to drive the disease in P1 and her father (**Fig E3**, *A-E*). In keeping, structure analysis predicted the extracellular R128K FAS mutation to be functionally conservative **(Fig E3**, *E*)

The R580Q variant reduces DSB ligation and DNA binding

The clinical phenotype of the *LIG4* variant carriers pointed to a protein loss of function associated with the R580Q variant. We performed substrate ligation assays comparing the enzymatic activity of recombinant wild-

type (WT) *vs.* mutant (R580Q) LIG4 protein **(Fig 4, *A*)**. As substrate, a 42 base pairs nicked oligonucleotide duplex (42mer) with attached fluorescent dye was used **(Fig 4, *B*)**. Applying increasing substrate concentration **(Fig 4, *C*)** and reaction duration **(Fig 4, *D*)** we observed reduced amounts of ligated products in the R580Q LIG4 presence as compared to WT.

Reduced biochemical ligation activity of the mutant R580Q LIG4 prompted us to study the LIG4-DNA interaction at the structural level. We performed molecular dynamics simulations, an approach allowing to efficiently interpret the effect of mutations on protein function[8, 20, 21]. The simulations focused on the catalytic domain of LIG4 in closed conformation with a nicked adenylated-DNA substrate (PDB 6BKG). Twelve independent unbiased trajectories of > 500ns, six for the WT and six for the R580Q mutant were computed. The Arg580 interacts with the broken 5' AMP-carrying DNA strand, with its guanidium moiety at a salt bridge distance from two phosphate groups **(Fig 4, *E*)** likely stabilizing the protein-DNA complex. Using the Molecular Mechanics Poisson–Boltzmann Surface Area (MMPBSA) approach[22-24], we calculated the free binding energy between the WT *vs.* R580Q LIG4 to the DNA. We found that the binding energy was lower in the case of the R584Q ligand **(Fig 4, *F* and *G*, Fig E4, *A* and *B*)**. The weakened R580Q LIG4-DNA binding could not be compensated by any of the 632 neighboring residues **(Fig E4, *B*)**. Thus, the residue 580 accounted alone for the largest binding energy (BE) reduction.

Next, we focused the conformational analysis on the interactions of the residue with the DNA backbone and on their torsion angles. The dihedral $\chi 1$ angle indicates the orientation of the sidechain with respect to the protein mainchain. The WT Arg580 experienced negligible oscillations in all trajectories, while the mutant Gln580 displayed greater dihedral $\chi 1$ angle fluctuations including a bimodal $\chi 1$ angle orientation **(Fig 4, *H* and *I*)**. This suggested that Gln580 was still sampling new conformations after 500ns. The fluctuations of Gln580 affected the secondary structure, causing a strong increase of the backbone torsion angles ϕ and ψ dynamics **(Fig E4, *C* – *F*)**. Quantification of either the salt bridges and hydrogen bonds formed between WT Arg580 respectively mutant Gln580 and the DNA **(Fig 4, *J*-*L*)**, disclosed a higher abundance of salt-bridges being formed for the WT **(Fig 4, *M*, Fig E4, *G*)**, significantly outnumbering the weaker hydrogen bonds for the mutant R580Q with the DNA **(Fig 4, *M*, Fig E4, *H*, video E1)**.

Several mutations affecting the LIG4 catalytic domain have been reported. We wondered whether any of the previously reported mutations **(Table I)** would be related to DNA binding, similarly to the one characterized here. The location of all human missense mutations affecting the LIG4 catalytic domain was compared to those of the trajectories in which the distance between enzyme and DNA was ≤ 3Å. Three residues other than the Arg580 were identified: p.278, p.447 and p.449 **(Fig 4, *N*)**. The positions p.278 and p.449 are well-described ATP-binding residues and a biochemical characterization for the p.447 mutation was not found in the literature. Consequently, the here described mutation at p.580 is to our knowledge the first with experimental evidence for reduced LIG4-DNA binding.

<u>Dysregulated DSB repair response in heterozygous *LIG4* mutated primary T cells</u>

To experimentally address LIG4 functionality in the context of a heterozygous missense variant, we characterized the DSB response in T cells of the patients *in vitro*.

After two days of *in vitro* culture, we observed spontaneously increased phosphorylation of two important DNA damage associated proteins H2Ax (γH2Ax) and 53BP1 (p53BP1)[25, 26] in T cells of both *LIG4* variant carriers **(Fig 5, *A* and *B*)**. Next, we measured nuclear γH2Ax kinetics after DSB induction *via* ionizing radiation (IR). Memory $CD45R0^+CD4^+$ T cells of both patients displayed higher $\gamma H2Ax^+$ levels beyond 48 hours after IR compared to cells from HDs **(Fig 5, *C*)**. The father's memory $CD45R0^+CD4^+$ T cells showed a trend and P1's memory $CD4^+$ T cells a distinctly augmented proportion H2Ax phosphorylation after *in vitro* treatment of PBMCs with the DSB inducing drug Bleomycin sulfate[27] **(Fig 5, *D*)**. This was paralleled by reduced cell viability

after *in vitro* Bleomycin sulfate exposure in naïve ($CD45R0^-$) and memory ($CD45R0^+$) $CD4^+$ T cells of both patients as compared to cells of HDs **(Fig 5, *E*)**.

T cell proliferation capacity after IR plus mitogen stimulation, was studied by labelling peripheral blood-derived T cells with CellTrace™ violet (CTV). Proliferation was quantified by assessing the CTV dye dilution. With rising IR-doses, we observed a trend for a decreased relative proliferation index in both $CD4^+$ and $CD8^+$ T cells of the two *LIG4* variant carriers compared to healthy T cells **(Fig 5, *F* and *G*)**.

The monoallelic LIG4 mutation p.A842D recapitulates impaired T-cell intrinsic DNA damage response and is linked with combined immunodeficiency

In our cohort of patients with immunodeficiency/immune-dysregulation, we identified two additional unrelated patients (P3 and P4), carrying an another functionally so far unstudied monoallelic *LIG4* mutation encoding p.A842D **(Fig 6, *A* and Table E2)**. Rare variants in other IEI-related genes filtered by WES in P3 and P4 were listed as benign or variant of unknown significance (VUS) on gnomAD/ClinVar and did not align with reported clinical features or zygosity reported by the international union of immunologic societies (IUIS)[28]. Both were adult patients with hypogammaglobulinemia, both sharing reduced naïve $CD4^+$ T cells with the LIG4 p.R580Q mutation carriers of the index family **(Table EI)**.

The alanine at position 842 is being conserved across species **(Fig 6, *B*)** within the BRCT2 domain of LIG4 interacting with its cofactor XRCC4 **(Fig 6, *C*)**. The distance of the proximal XRCC4 residues (Gln159, Glu163 and Val166) and LIG4 is exceeding 8Å in a reported 2.4 Å resolution model centered around the LIG4 BRCT segment-XRCC4 interaction (PDB 3II6) implying an indirect influence of the A842D substitution on molecular interaction[29]. We conducted 500 ns long independent unbiased MD trajectories, four of the WT and four of the A842D variant. The analyses focused on residues located within a range of 15Å of the Cα atom of residue 842 **(Fig 6, *C* and Fig E5)**. Results delineated potential alteration of a network of salt bridges involving multiple residues of XRCC4 and BRCT. A domino-effect of the A842D mutation was predicted to skew four pairs of acidic and basic residues located in BRCT2 and XRCC4 **(Fig E5)**. These changes are predicted to shift binding along the XRCC4 helices (see legend of **Fig E5** for detailed description). The effect of the A842D mutation was conceptually analogous to a XRCC4 R161Q mutation causing reduced DNA repair[30].

We next re-addressed immune cell-intrinsic consequences of both R580Q and A842D mutations in heterozygous state in primary T cells. Bleomycin treatment of PBMCs derived from A842D-mutated P3 and P4 resulted in significantly elevated $CD3^+$ T cell death equivalent to re-analyzed R580Q-mutated P1 **(Fig 6, *D* and *E*)**. TCR $V\alpha7.2^+$ frequencies in T cells **(Table EI** and **Fig 6, *F*)** were low similar to P1 **(Fig 6, *G*)**. When $V\alpha7.2^+$ TCR frequencies and T cell bleomycin induced cell death rates were correlated, two-dimensional plotting resulted in a distinct segregation of *LIG4*-mutated patients P1, P3 and P4 with healthy control and also with unrelated immune disease patients **(Fig 6, *H*)**. When the slope of (% bleomycin-induced cell death)/(% $V\alpha7.2^+$) was computed for each individual, this T-cell functional index distinctly differentiated LIG4-mutated patients from all other individuals examined **(Fig 6, *H*)**. Subset-level analysis of bleomycin-induced cell death in $CD4^+$ T cells showed for naïve $CD4^+$ T cells a notable acceleration **(Fig E6, *A*)**. This was in keeping with the low *ex vivo* frequencies of this subset as naïve $CD4^+$ T-cell frequencies were lower and central memory $CD4^+$ T-cell frequencies reciprocally higher in patients P1-P4 compared with examined healthy and disease controls **(Fig E6, *B-D*)**.

In summary, accelerated DNA damage-induced T-cell death is a common feature in the currently identified heterozygous LIG4 R580Q and A842D monoallelic mutated patients.

LIG4 R580Q and A842D mutations are functionally haploinsufficient

We next addressed the T cell-intrinsic consequences of the LIG4 R580Q and A842D mutations by reconstituting LIG4 in a newly generated *LIG4*-knock-out (*LIG4*-KO) Jurkat T-cell line. Using the CRISPR-Cas9 system we generated Jurkat T cells carrying a frameshift mutation in the *LIG4* gene resulting in LIG4 loss of expression as confirmed by western blot and flow cytometry **(Fig 7, *A*)**. Bleomycin treatment of *LIG4*-KO Jurkat T cells cells resulted in augmented apoptosis in a dose- and time-dependent manner as compared with LIG4 competent cells **(Fig 7, *B* and *C*)**, functionally verifying that tolerance towards DNA damage is LIG4 dependent.

We next designed a transient transfection/overexpression-based LIG4 reconstitution in the *LIG4*-KO Jurkat T cells **(Fig 7, *D*, top left)**. A combined usage of a cationic polymer with magnetofection reproducibly attained reporter protein/LIG4 protein-positive populations **(Fig 7, *D*, left bottom)**. This occurred with a low basal cytotoxicity enabling quantitative analysis upon *in vitro* DNA damage induced by bleomycin. Wild type (WT) LIG4-expressing Jurkat T cells typically demonstrated a rescue from cell death which was not observed in R580Q and A842D LIG4 reconstituted cells **(Fig 7, *D and E*)**. There was certain inter-assay variability in these complex reconstitution experiments whereas genotype differences (WT *vs.* MUT) were consistent. Thus, both LIG4 mutant proteins are loss of function in this reconstitution system.

A mixed reconstitution of WT and R580Q or A842D LIG4 did not significantly alter T cell apoptosis compared to reconstitution with WT alone **(Fig 7, *F*)**, even when using a 3:1 ratio in favor of the mutant LIG4. These results rule out a dominant negative function of the R580Q and the A842D LIG4 variants.

In summary, the LIG4 R580Q and A842D mutations are loss of function causing LIG4 haploinsufficiency upon DNA damage when present in heterozygous state.

Discussion

The clinical phenotype of human LIG4 deficiency is broad, ranging from asymptomatic carriers to death *in utero* **(Table I).** To our knowledge, all LIG4 deficient patients described so far carried homozygous or compound heterozygous *LIG4* mutations. However, Rucci et al. described reduced survival in mice carrying a heterozygous *Lig4* missense mutation[6]. The immune-phenotype and clinical status of parents or siblings of published LIG4 deficient patients has not been studied systematically yet, albeit collective experience suggests immune-competence in those monoallelic LIG4^{mut} carriers.

All four patients with monoallelic novel *LIG4* mutations characterized here had hypogamma–globulinemia, low naïve CD4^{+} T cells, low Vα7.2 TCR segment usage and displayed augmented T cell intrinsic cell death upon bleomycin exposure. T cell intrinsic hypersensitivity to experimental DNA damage in the four heterozygous *LIG4* mutation carriers analyzed here is a key characteristic in LIG4 deficiency[31].

The diversified TCR repertoire in both heterozygous *LIG4* mutation carriers analyzed is in keeping with TCR repertoire analysis of published patients with compound heterozygous *LIG4* mutations[32-35]. These similarities between published biallelic and the here presented monoallelic *LIG4* mutation carriers might be explained by by the degree of functional hypomorphism[31]. This has however not been studied so far. Besides the role for LIG4 in thymic T cell development, resting peripheral T cells have been found to be particularly sensitive to DNA damage[36], possibly contributing to the observed low naïve T cell frequencies in heterozygous *LIG4* mutation carriers.

We have documented immunodeficiency, lymphoproliferation and autoimmunity in the patients analyzed here, including unique complications not yet documented in association with *LIG4* deficiency. However, the full clinical spectrum associated with LIG4 haploinsufficiency is predicted to widen as more patients are identified[37, 38]. We can currently not conclude on the clinical penetrance of LIG4 haploinsufficiency. Penetrance and also clinical phenotypes are known to be modified by environmental influence (e.g. immune-suppressive treatment or recurrent x-ray based imaging in P1), epigenetics and also rare germline variants in other immune-system genes[39].

Our newly established transfection platform to test functionality of identified rare *LIG4* variants, in combination with molecular dynamic simulations, may guide definitive molecular diagnosis in possible LIG4 haploinsufficiency.

In summary, this is to our knowledge the first report of LIG4 haploinsufficiency associated with monoallelic *LIG4* mutations, driving human immune-dysregulatory disease that may segregate as an autosomal dominant trait. In patients with immune-dysregulation of unknown cause, we encourage to consider LIG4 haploinsufficiency as it may have specific prognostic and therapeutic consequences.

Acknowledgments

We thank the patients and their families, the Department of Biomedicine core facilities, the University Hospital Basel and Blood Donor Center Basel. We thank Primo Schär, University of Basel, Switzerland for advice regarding the ligation assay.

References

1. Caron P, van der Linden J, van Attikum H. Bon voyage: A transcriptional journey around DNA breaks. DNA Repair (Amst). 2019;82:102686.
2. Chang HHY, Pannunzio NR, Adachi N, Lieber MR. Non-homologous DNA end joining and alternative pathways to double-strand break repair. Nat Rev Mol Cell Biol. 2017;18(8):495-506.
3. Notarangelo LD, Kim MS, Walter JE, Lee YN. Human RAG mutations: biochemistry and clinical implications. Nat Rev Immunol. 2016;16(4):234-46.
4. Frank KM, Sekiguchi JM, Seidl KJ, Swat W, Rathbun GA, Cheng HL, et al. Late embryonic lethality and impaired V(D)J recombination in mice lacking DNA ligase IV. Nature. 1998;396(6707):173-7.
5. Sharpless NE, Ferguson DO, O'Hagan RC, Castrillon DH, Lee C, Farazi PA, et al. Impaired Nonhomologous End-Joining Provokes Soft Tissue Sarcomas Harboring Chromosomal Translocations, Amplifications, and Deletions. Molecular Cell. 2001;8(6):1187-96.
6. Rucci F, Notarangelo LD, Fazeli A, Patrizi L, Hickernell T, Paganini T, et al. Homozygous DNA ligase IV R278H mutation in mice leads to leaky SCID and represents a model for human LIG4 syndrome. Proc Natl Acad Sci U S A. 2010;107(7):3024-9.
7. Navarini AA, Hruz P, Berger CT, Hou TZ, Schwab C, Gabrysch A, et al. Vedolizumab as a successful treatment of CTLA-4-associated autoimmune enterocolitis. J Allergy Clin Immunol. 2017;139(3):1043-6 e5.
8. Burgener AV, Bantug GR, Meyer BJ, Higgins R, Ghosh A, Bignucolo O, et al. SDHA gain-of-function engages inflammatory mitochondrial retrograde signaling via KEAP1-Nrf2. Nat Immunol. 2019;20(10):1311-21.
9. Chitty-Lopez M, Westermann-Clark E, Dawson I, Ujhazi B, Csomos K, Dobbs K, et al. Asymptomatic Infant With Atypical SCID and Novel Hypomorphic RAG Variant Identified by Newborn Screening: A Diagnostic and Treatment Dilemma. Front Immunol. 2020;11:1954.
10. Berland A, Rosain J, Kaltenbach S, Allain V, Mahlaoui N, Melki I, et al. PROMIDISalpha: A T-cell receptor alpha signature associated with immunodeficiencies caused by V(D)J recombination defects. J Allergy Clin Immunol. 2019;143(1):325-34 e2.
11. Shannon CE. The mathematical theory of communication. 1963. MD Comput. 1997;14(4):306-17.
12. Simpson EH. Measurement of Diversity. Nature. 1949;163(4148):688-.
13. Kumar BV, Connors TJ, Farber DL. Human T Cell Development, Localization, and Function throughout Life. Immunity. 2018;48(2):202-13.
14. Uduman M, Shlomchik MJ, Vigneault F, Church GM, Kleinstein SH. Integrating B cell lineage information into statistical tests for detecting selection in Ig sequences. J Immunol. 2014;192(3):867-74.
15. Ghraichy M, Galson JD, Kovaltsuk A, von Niederhausern V, Pachlopnik Schmid J, Recher M, et al. Maturation of the Human Immunoglobulin Heavy Chain Repertoire With Age. Front Immunol. 2020;11:1734.
16. Kaminski AM, Tumbale PP, Schellenberg MJ, Williams RS, Williams JG, Kunkel TA, et al. Structures of DNA-bound human ligase IV catalytic core reveal insights into substrate binding and catalysis. Nat Commun. 2018;9(1):2642.
17. Kircher M, Witten DM, Jain P, O'Roak BJ, Cooper GM, Shendure J. A general framework for estimating the relative pathogenicity of human genetic variants. Nat Genet. 2014;46(3):310-5.
18. Adzhubei IA, Schmidt S, Peshkin L, Ramensky VE, Gerasimova A, Bork P, et al. A method and server for predicting damaging missense mutations. Nat Methods. 2010;7(4):248-9.
19. Kumar P, Henikoff S, Ng PC. Predicting the effects of coding non-synonymous variants on protein function using the SIFT algorithm. Nat Protoc. 2009;4(7):1073-81.
20. Bignucolo O, Leung HT, Grzesiek S, Berneche S. Backbone hydration determines the folding signature of amino acid residues. J Am Chem Soc. 2015;137(13):4300-3.
21. Bignucolo O, Vullo S, Ambrosio N, Gautschi I, Kellenberger S. Structural and Functional Analysis of Gly212 Mutants Reveals the Importance of Intersubunit Interactions in ASIC1a Channel Function. Front Mol Biosci. 2020;7:58.

22. Srinivasan J, Cheatham TE, Cieplak P, Kollman PA, Case DA. Continuum Solvent Studies of the Stability of DNA, RNA, and Phosphoramidate−DNA Helices. Journal of the American Chemical Society. 1998;120(37):9401-9.
23. Kumari R, Kumar R, Open Source Drug Discovery C, Lynn A. g_mmpbsa--a GROMACS tool for high-throughput MM-PBSA calculations. J Chem Inf Model. 2014;54(7):1951-62.
24. Baker NA, Sept D, Joseph S, Holst MJ, McCammon JA. Electrostatics of nanosystems: application to microtubules and the ribosome. Proc Natl Acad Sci U S A. 2001;98(18):10037-41.
25. Rogakou EP, Pilch DR, Orr AH, Ivanova VS, Bonner WM. DNA double-stranded breaks induce histone H2AX phosphorylation on serine 139. J Biol Chem. 1998;273(10):5858-68.
26. Panier S, Boulton SJ. Double-strand break repair: 53BP1 comes into focus. Nat Rev Mol Cell Biol. 2014;15(1):7-18.
27. Steighner RJ, Povirk LF. Bleomycin-induced DNA lesions at mutational hot spots: implications for the mechanism of double-strand cleavage. Proc Natl Acad Sci U S A. 1990;87(21):8350-4.
28. Tangye SG, Al-Herz W, Bousfiha A, Cunningham-Rundles C, Franco JL, Holland SM, et al. Human Inborn Errors of Immunity: 2022 Update on the Classification from the International Union of Immunological Societies Expert Committee. J Clin Immunol. 2022;42(7):1473-507.
29. Menchon G, Bombarde O, Trivedi M, Negrel A, Inard C, Giudetti B, et al. Structure-Based Virtual Ligand Screening on the XRCC4/DNA Ligase IV Interface. Sci Rep. 2016;6:22878.
30. Rosin N, Elcioglu NH, Beleggia F, Isguven P, Altmuller J, Thiele H, et al. Mutations in XRCC4 cause primary microcephaly, short stature and increased genomic instability. Hum Mol Genet. 2015;24(13):3708-17.
31. Altmann T, Gennery AR. DNA ligase IV syndrome; a review. Orphanet J Rare Dis. 2016;11(1):137.
32. Felgentreff K, Baxi SN, Lee YN, Dobbs K, Henderson LA, Csomos K, et al. Ligase-4 Deficiency Causes Distinctive Immune Abnormalities in Asymptomatic Individuals. J Clin Immunol. 2016;36(4):341-53.
33. Enders A, Fisch P, Schwarz K, Duffner U, Pannicke U, Nikolopoulos E, et al. A severe form of human combined immunodeficiency due to mutations in DNA ligase IV. J Immunol. 2006;176(8):5060-8.
34. Buck D, Moshous D, de Chasseval R, Ma Y, le Deist F, Cavazzana-Calvo M, et al. Severe combined immunodeficiency and microcephaly in siblings with hypomorphic mutations in DNA ligase IV. Eur J Immunol. 2006;36(1):224-35.
35. Luo X, Liu Q, Jiang J, Tang W, Ding Y, Zhou L, et al. Characterization of a Cohort of Patients With LIG4 Deficiency Reveals the Founder Effect of p.R278L, Unique to the Chinese Population. Front Immunol. 2021;12:695993.
36. Hu Q, Xie Y, Ge Y, Nie X, Tao J, Zhao Y. Resting T cells are hypersensitive to DNA damage due to defective DNA repair pathway. Cell Death Dis. 2018;9(6):662.
37. Delmonte OM, Schuetz C, Notarangelo LD. RAG Deficiency: Two Genes, Many Diseases. J Clin Immunol. 2018;38(6):646-55.
38. Walter JE, Ziegler JB, Ballow M, Cunningham-Rundles C. Advances and Challenges of the Decade: The Ever-Changing Clinical and Genetic Landscape of Immunodeficiency. J Allergy Clin Immunol Pract. 2023;11(1):107-15.
39. Gruber C, Bogunovic D. Incomplete penetrance in primary immunodeficiency: a skeleton in the closet. Hum Genet. 2020;139(6-7):745-57.
40. Rowe JH. Abnormalities of T-cell receptor repertoire in CD41 regulatory and conventional T cells in patients with RAG mutations: Implications for autoimmunity. Journal of Allergy and Clinical Immunology. 2017.
41. Bashford-Rogers RJM, Bergamaschi L, McKinney EF, Pombal DC, Mescia F, Lee JC, et al. Analysis of the B cell receptor repertoire in six immune-mediated diseases. Nature. 2019;574(7776):122-6.
42. Sharapova SO, Chang EY, Guryanova IE, Proleskovskaya IV, Fedorova AS, Rutskaya EA, et al. Next generation sequencing revealed DNA ligase IV deficiency in a "developmentally normal" patient with massive brain Epstein-Barr virus-positive diffuse large B-cell lymphoma. Clin Immunol. 2016;163:108-10.

43. Staines Boone AT, Chinn IK, Alaez-Verson C, Yamazaki-Nakashimada MA, Carrillo-Sanchez K, Garcia-Cruz MLH, et al. Failing to Make Ends Meet: The Broad Clinical Spectrum of DNA Ligase IV Deficiency. Case Series and Review of the Literature. Front Pediatr. 2018;6:426.
44. Castro ACE, Maia R, Batalha S, Freixo JP, Martins C, Neves C, et al. Case Report: Wide Spectrum of Manifestations of Ligase IV Deficiency: Report of 3 Cases. Front Immunol. 2022;13:869728.
45. Madhu R, Beaman GM, Chandler KE, O'Sullivan J, Urquhart JE, Khan N, et al. Ligase IV syndrome can present with microcephaly and radial ray anomalies similar to Fanconi anaemia plus fatal kidney malformations. Eur J Med Genet. 2020;63(9):103974.
46. IJspeert H, Warris A, van der Flier M, Reisli I, Keles S, Chishimba S, et al. Clinical spectrum of LIG4 deficiency is broadened with severe dysmaturity, primordial dwarfism, and neurological abnormalities. Hum Mutat. 2013;34(12):1611-4.
47. Murray JE, Bicknell LS, Yigit G, Duker AL, van Kogelenberg M, Haghayegh S, et al. Extreme growth failure is a common presentation of ligase IV deficiency. Hum Mutat. 2014;35(1):76-85.
48. Schober S, Schilbach K, Doering M, Cabanillas Stanchi KM, Holzer U, Kasteleiner P, et al. Allogeneic hematopoietic stem cell transplantation in two brothers with DNA ligase IV deficiency: a case report and review of the literature. BMC Pediatr. 2019;19(1):346.
49. Opitz JM, Pfeiffer RA, Hermann JP, Kushnick T. Studies of malformation syndromes of man XXIV B: the Dubowitz syndrome. Further observations. Z Kinderheilkd. 1973;116(1):1-12.
50. Yue J, Lu H, Lan S, Liu J, Stein MN, Haffty BG, et al. Identification of the DNA repair defects in a case of Dubowitz syndrome. PLoS One. 2013;8(1):e54389.
51. Toita N, Hatano N, Ono S, Yamada M, Kobayashi R, Kobayashi I, et al. Epstein-Barr virus-associated B-cell lymphoma in a patient with DNA ligase IV (LIG4) syndrome. Am J Med Genet A. 2007;143A(7):742-5.
52. Matsumoto K, Hoshino A, Nishimura A, Kato T, Mori Y, Shimomura M, et al. DNA Ligase IV Deficiency Identified by Chance Following Vaccine-Derived Rubella Virus Infection. J Clin Immunol. 2020;40(8):1187-90.
53. Dobbs K, Tabellini G, Calzoni E, Patrizi O, Martinez P, Giliani SC, et al. Natural Killer Cells from Patients with Recombinase-Activating Gene and Non-Homologous End Joining Gene Defects Comprise a Higher Frequency of CD56(bright) NKG2A(+++) Cells, and Yet Display Increased Degranulation and Higher Perforin Content. Front Immunol. 2017;8:798.
54. Riballo E, Doherty AJ, Dai Y, Stiff T, Oettinger MA, Jeggo PA, et al. Cellular and biochemical impact of a mutation in DNA ligase IV conferring clinical radiosensitivity. J Biol Chem. 2001;276(33):31124-32.
55. O'Driscoll M, Cerosaletti KM, Girard P-M, Dai Y, Stumm M, Kysela B, et al. DNA Ligase IV Mutations Identified in Patients Exhibiting Developmental Delay and Immunodeficiency. Molecular Cell. 2001;8(6):1175-85.
56. Girard PM, Kysela B, Harer CJ, Doherty AJ, Jeggo PA. Analysis of DNA ligase IV mutations found in LIG4 syndrome patients: the impact of two linked polymorphisms. Hum Mol Genet. 2004;13(20):2369-76.
57. Slack J, Albert MH, Balashov D, Belohradsky BH, Bertaina A, Bleesing J, et al. Outcome of hematopoietic cell transplantation for DNA double-strand break repair disorders. J Allergy Clin Immunol. 2018;141(1):322-8 e10.
58. Plowman PN, Bridges BA, Arlett CF, Hinney A, Kingston JE. An instance of clinical radiation morbidity and cellular radiosensitivity, not associated with ataxia-telangiectasia. Br J Radiol. 1990;63(752):624-8.
59. Riballo E, Critchlow SE, Teo SH, Doherty AJ, Priestley A, Broughton B, et al. Identification of a defect in DNA ligase IV in a radiosensitive leukaemia patient. Current Biology. 1999;9(13):699-S2.
60. Cifaldi C AG, Chiriaco M, Di Cesare S, Claps A, Serafinelli J, Rossi P, Antoccia A, Di Matteo G, Cancrini C, De Villartay JP, Finocchi A. Late-onset combined immune deficiency due to LIGIV mutations in a 12-year-old patient. Pediatr Allergy Immunol. 2017;28(2):201-3.
61. Jiang J, Tang W, An Y, Tang M, Wu J, Qin T, et al. Molecular and immunological characterization of DNA ligase IV deficiency. Clin Immunol. 2016;163:75-83.
62. Sun B, Chen Q, Wang Y, Liu D, Hou J, Wang W, et al. LIG4 syndrome: clinical and molecular characterization in a Chinese cohort. Orphanet J Rare Dis. 2020;15(1):131.
63. Huang M, Dong G, Lu X, Xiao F, Zhou Q, Zhang S. DNA ligase IV dificiency with elevated serum IgG levels suspected to have myelodysplastic syndrome: a case report. BMC Pediatr. 2022;22(1):588.

64. Slatter MA, Gennery AR. Update on DNA-Double Strand Break Repair Defects in Combined Primary Immunodeficiency. Curr Allergy Asthma Rep. 2020;20(10):57.
65. Grunebaum E BA, Roifman C. Omenn syndrome is associated with mutations in DNA ligase IV. J Allergy Clin Immunol. 2008;122(6):1219-20.
66. Bluteau O, Sebert M, Leblanc T, Peffault de Latour R, Quentin S, Lainey E, et al. A landscape of germ line mutations in a cohort of inherited bone marrow failure patients. Blood. 2018;131(7):717-32.
67. Dard R, Herve B, Leblanc T, de Villartay JP, Collopy L, Vulliami T, et al. DNA ligase IV deficiency: Immunoglobulin class deficiency depends on the genotype. Pediatr Allergy Immunol. 2017;28(3):298-303.
68. Brunet BA, Dave N. Unique heterozygous presentation in an infant with DNA ligase IV syndrome. Ann Allergy Asthma Immunol. 2017;119(4):379-80.
69. Liao W, Ngan BY, Merico D, Dadi H, Roifman CM. A novel mutation in LIG4 in an infant presenting with severe combined immunodeficiency with thymic medullary dysplasia. LymphoSign Journal. 2017.
70. Buchbinder D, Hauck F, Albert MH, Rack A, Bakhtiar S, Shcherbina A, et al. Rubella Virus-Associated Cutaneous Granulomatous Disease: a Unique Complication in Immune-Deficient Patients, Not Limited to DNA Repair Disorders. J Clin Immunol. 2019;39(1):81-9.
71. Tamura S, Higuchi K, Tamaki M, Inoue C, Awazawa R, Mitsuki N, et al. Novel compound heterozygous DNA ligase IV mutations in an adolescent with a slowly-progressing radiosensitive-severe combined immunodeficiency. Clin Immunol. 2015;160(2):255-60.
72. van der Burg M, van Veelen LR, Verkaik NS, Wiegant WW, Hartwig NG, Barendregt BH, et al. A new type of radiosensitive T-B-NK+ severe combined immunodeficiency caused by a LIG4 mutation. J Clin Invest. 2006;116(1):137-45.
73. Fadda A, Butt F, Tomei S, Deola S, Lo B, Robay A, et al. Two hits in one: whole genome sequencing unveils LIG4 syndrome and urofacial syndrome in a case report of a child with complex phenotype. BMC Med Genet. 2016;17(1):84.
74. O'Driscoll M, Gennery AR, Seidel J, Concannon P, Jeggo PA. An overview of three new disorders associated with genetic instability: LIG4 syndrome, RS-SCID and ATR-Seckel syndrome. DNA Repair (Amst). 2004;3(8-9):1227-35.
75. Gruhn B, Seidel J, Zintl F, Varon R, Tonnies H, Neitzel H, et al. Successful bone marrow transplantation in a patient with DNA ligase IV deficiency and bone marrow failure. Orphanet J Rare Dis. 2007;2:5.
76. Zhang MY, Keel SB, Walsh T, Lee MK, Gulsuner S, Watts AC, et al. Genomic analysis of bone marrow failure and myelodysplastic syndromes reveals phenotypic and diagnostic complexity. Haematologica. 2015;100(1):42-8.
77. Unal S, Cerosaletti K, Uckan-Cetinkaya D, Cetin M, Gumruk F. A novel mutation in a family with DNA ligase IV deficiency syndrome. Pediatr Blood Cancer. 2009;53(3):482-4.
78. Chadha P, Thibodeau R, Jafroodifar A, Majmudar A. A case report of an adolescent with ligase-4 deficiency and the potential dangers of ionizing radiation in this rare patient population. Radiol Case Rep. 2021;16(10):2890-3.
79. Ben-Omran TI, Cerosaletti K, Concannon P, Weitzman S, Nezarati MM. A patient with mutations in DNA Ligase IV: clinical features and overlap with Nijmegen breakage syndrome. Am J Med Genet A. 2005;137A(3):283-7.
80. Taskiran EZ, Sonmez HE, Kosukcu C, Tavukcuoglu E, Yazici G, Esendagli G, et al. A Novel Missense LIG4 Mutation in a Patient With a Phenotype Mimicking Behcet's Disease. J Clin Immunol. 2019;39(1):99-105.
81. Hayani A, Suarez CR, Molnar Z, LeBeau M, Godwin J. Acute myeloid leukaemia in a patient with Seckel syndrome. J Med Genet. 1994;31(2):148-9.
82. Straathof KC, Rao K, Eyrich M, Hale G, Bird P, Berrie E, et al. Haemopoietic stem-cell transplantation with antibody-based minimal-intensity conditioning: a phase 1/2 study. The Lancet. 2009;374(9693):912-20.

Figure legends

FIG. 1| Multiple autoimmune manifestations and reduction of naïve T cells in the peripheral blood of P1 and her father. A) Clinical manifestations in the index patient P1, thrombocyte counts, hemoglobin levels, grey background depicts reference range. Ears nose throat ENT, varicella-zoster virus VZV. **B)** P1's kidney biopsy during interstitial nephritis. Immunohistochemistry staining with anti-CD20 and anti-CD4. **C)** Pulmonary tissue gated computer tomography scan of P1 during the pneumonitis episode and **D)** after steroid treatment. **E)** Lung biopsy specimens during the pneumonitis episode and stained with anti-CD20 and anti-CD3. **F)** Cranial magnetic resonance imaging, showing parotid gland swelling (white arrowheads). **G)** Peripheral blood T cell subsets with naïve ($CD27^+CD45RO^-$), effector memory (EM, $CD27^-CD45RO^+$) and central memory (CM, $CD27^+CD45RO^+$) and **H)** quantification. **I)** CellTrace™ violet (CTV) dilution after 5 days of *in vitro* stimulation. **J)** Enumeration of T cells bearing the TCR Vα7.2 segment by flow-cytometry. The number indicates the frequency within the $CD3^+$ T cell population. **K)** Comparison of the TCR V$\alpha7.2^+$ T cell frequency in P1 and her father with patients affected by combined immunodeficiency (CID), primary antibody deficiency (PAD), autoinflammation (Autoinflamm.) or to healthy donors (HD). (K) non-parametric Kruskal-Wallis test with Dunn's correction ** $p<0.01$.

FIG. 2| Preserved B and T cell receptor repertoires. A) High throughput sequencing of the T cell receptor loci. CDR3 length distribution. **B)** Shannon's (H) entropy index, grey shadow for HD values[40]. **C)** Simpson clonality index. **D)** Individual *V* gene segment usage. **E)** Heatmaps displaying *VJ* gene pairing, box indicates most distal gene pairing. **F)** Surface expression of the BCR light chains. **G)** *IGH* locus cartoon for the constant region (adapted from[41]). *IGH* high-throughput RNA sequencing for the determination of B cell maturation status and constant region gene usage. **H)** IgA and IgG subclass utilization. Box-plot indicates age-matched HDs values. **I)** V family and **(J)** J gene segment usage. Box-plot indicates values of age-matched HDs. **K)** Average of somatic hypermutations (SHM). The black line indicates the model fitting the SHM increase by age, gray lines indicate the 95% confidence interval. **L)** Antigen selection was quantified by the computation of the mean replacement/silent (R/S) ratio. The black line indicates the model fitting, the R/S increase by age, gray lines indicate the 95% confidence interval. (D) differential expression analysis empirical Bayes method. (F) Mann-Whitney test with post-hoc correction, the HDs SD was added to the value of P1.

FIG. 3|Novel missense variant within the catalytic core of DNA ligase 4. **A)** Sanger sequencing of c.A1739G in bulk T cell-derived DNA, the resulting amino acid change at p.R580Q is indicated. **B)** Multiple LIG4 protein sequence alignment, p.580 position is highlighted. **C)** Molecular representation in ribbons of the human LIG4 catalytic core bound to a DNA duplex. The WT Arg580 is shown as stick (arrow). The corresponding β sheet 18 is indicated. The mutated amino acid resides in the catalytic oligonucleotide/oligosaccharide-fold domain (OBD, blue). Numbers indicate the amino acid position in NP_001091738. BRCT1: BRCA1 C terminus; BRCT2: BRCA2 C terminus; DBD DNA binding domain in green; NTD nucleotidyltransferase in orange. **D)** Qualitative polymerase chain reaction (qPCR) was used to measure *LIG4* mRNA levels in PBMCs of the two patients and healthy controls including the mother. The relative quantity (RQ) was normalized to multiple housekeeping genes and to the mean of the HDs. **E)** The LIG4 protein levels were quantified by separating PHA T cell blast cell lysates by SDS-PAGE electrophoresis and probed with rabbit-anti LIG4. Right side normalization of LIG4 protein levels to β-actin levels. (d) non-parametric Mann-Whitney rank test, ns not significant.

FIG. 4| LIG4 R580Q reduces DNA-ligation activity and weakens DNA-binding. A) Normalization of recombinant WT or R580Q LIG4 proteins. **B)** 42mer nicked DNA-duplex. Multiple turnover-ligations for WT *vs.* R580Q LIG4 with **C)** increasing unadenylated 42mer concentrations and **d)** time. Product separation on a TBE-Urea polyacrylamide gel. **E)** Molecular OBD representation, the Arg580 represented as stick (arrows: nearby DNA-backbone phosphorous atoms). **F)** Computed LIG4 binding energy (BE) between the WT *vs.* R580Q LIG4 and adenylated-DNA complex. Twelve independent trajectories, each >500ns. **G)** Residues with BE difference >20 kJ/mol between WT and R580Q. **H)** Dihedral ?1 angle time series and **I)** distribution focused on residue 580. **(J)** WT LIG4 and **(K)** R580Q LIG4 (stick) with the adenylated nicked-DNA as ball and stick. 3rd and 4th phosphate group of DNA-backbone (arrows). **L)** Minimal distance between the residue sidechain and DNA-backbone phosphate groups. The phosphate group-numbering is indicated. **M)** Temporal fraction, during which residue 580 sidechain and the DNA-backbone phosphate were < 4 Å. **N)** Bottom: Identification of likely DNA-interacting residues (distance to DNA < 3 Å). Middle: Human *LIG4* missense mutations (Table I). Top: Missense mutations with potential DNA binding. Mann-Whitney testing (F) with multiple comparison correction (L), (G) 2wayANOVA with Šídàk correction.

FIG.5| Augmented DNA-damage susceptibility *in vitro*. T cells derived from PBMCs were cultured for two days without stimulation. The phosphorylation of H2Ax (γH2Ax) and 53BP1 (p53BP1) were assessed by flow cytometry. **A)** Quantification (mean of triplicates) and **(B)** representative flow cytometric plots of the γH2Ax^{+}p53BP1^{+} population in bulk CD3^{+} T cells. **C)** Kinetics of γH2Ax in CD45R0^{+}CD4^{+} helper T cells after 10Gy irradiation (IR). **D)** Analysis of the nuclear γH2Ax^{+} fraction in memory CD45R0^{+} CD4^{+} T cells after *in vitro*

treatment of PBMCs with Bleomycin sulfate for 24 hours at indicated concentrations. **E)** Cell death after 24 hours *in vitro* Bleomycin sulfate exposure of $CD4^+$ T cells (naïve $CD45R0^-$ and memory $CD45R0^+$). **F)** T cell proliferation after IR. T cells were labelled with CellTrace™ violet (CTV), followed by IR and stimulation for five days *in vitro* with anti-CD3/anti-CD28 (aCD3/aCD28). Gray shaded population indicates the maternal non-stimulated condition of T cells. **G)** The relative proliferation index was computed for $CD4^+$ and $CD8^+$ T cells after different IR intensities, stimulation of cells as in (F). (A) Kruskal-Wallis test, (C/D/E/G) 2wayANOVA with Šídàk correction. Single points represent mean values of duplicates or triplicates for the patients.

FIG. 6| A novel LIG4 A842D mutation substantiates linkage of monoallelic *LIG4* mutations with DNA damage-induced T-cell death and immunodeficiency. A) Sanger sequencing chromatogram of heterozygous LIG4 A842D mutation in P3 and P4. **B)** Cross-species alignment of A842-proximal LIG4 residues. **C)** LIG4-XRCC4 molecular complex highlighting residue 846-proximal area of BRCT2. Structural domains shown in black (BRCT1/BRCT2), blue (XRCC4-A) and red (XRCC4-B). Simulation snapshots in boxes for WT (top) and A842D (bottom) LIG4. Salt bridges shown as dashed lines when distances were mostly below 5Å during simulation. **D)** Dead cell stain-positive frequencies (mean ± SD) in T cells following 24-hour bleomycin exposure in blood-donors (n = 15, black), disease-controls (green) and patients P1 (R580Q), P3 and P4 (A842D). **E)** Post-hoc comparisons of one-way ANOVA for bleomycin-treated groups. Representative data shown as mean of pooled triplicate/quadruplicate (P1), duplicate/triplicate (P3) or triplicate/quadruplicate (P4). **F)** Flow-cytometric plots of TCRVα7.2$^+$ T cells. **G)** TCR Vα7.2$^+$ T cell frequencies of healthy controls (gray), disease-controls (green) and in LIG4-mutated patients (pink). **H)** Two-dimensional plot of *ex vivo* TCRVα7.2$^+$ versus *in vitro* 24-hour 50 µM bleomycin-induced T-cell death. An empirical slope of 2 is appended. **I)** One-way ANOVA of T cell-functionality slope defined as (24-hour bleomycin-induced dead frequencies)/(TCRVα7.2-positive frequencies).

FIG 7| LIG4 R580Q and A842D loss-of-function mutants manifest haploinsufficiency upon reconstitution. **A)** Verification of CRISPR-Cas9-mediated *LIG4* knockout in Jurkats (Top). LIG4-expression impairment was verified by intracellular staining (bottom left) and western blotting (bottom right). **B)** Flow-cytometric plots of WT (left) versus *LIG4*-knocked out (LIG4-KO) (right) Jurkat T-cells exposed to bleomycin (12 hours). **C)** Dose- (12h) and time- (50µM) dependent frequencies of Annexin V-positive apoptotic cell frequencies following bleomycin exposure. Performed in triplicate (0µM, 10µM) or quadruplicate (50µM) and compared by unpaired t-tests. **D)** LIG4 functional reconstitution schematic via transient overexpression in LIG4-KO Jurkat T-cells. Cells were magnetofected via cationic polymers with a dual-promoter, LIG4/mCherry co-expressing vector (representative flow plot: bottom), then exposed to bleomycin and evaluated for Annexin V positivity in

mCherry(/LIG4)-positive/negative populations. A representative calculation is shown. **E)** Comparison of post-bleomycin survival rates in mCherry+ cells normalized against intra-well mCherry- fractions upon WT versus mutant *LIG4* transfection. Representative of two independent experiments performed in quadruplicate. Compared by unpaired t-tests. **F)** Comparison of post-bleomycin incubation survival rates in mCherry+ cells upon WT and mutant LIG4 co-transfection at indicated ratios. Post-hoc comparisons of one-way ANOVA are shown. Pooled data of two independent experiments performed in triplicate/quadruplicate/control are shown (mean ± SEM).

704 **Table I**| Clinical and genetic features of published patients with confirmed *LIG4* mutation. Patients are ordered according to the 5' position of the first mutated allele. cDNA
705 sequence refers to NM_001098268.

c.C8T + c.C26T	c.2736+3delC	p.A3V + p.T9I	NA	Comp. het.	Additional polymorphisms in *ATM, NOD2, NLRP3*	none	(42)	R_001
c.C32G	c.T1236T	p.A11G	p.N412K	Comp. het.		none	(43)	R_002
c.C32G	c.T1236T	p.A11G	p.N412K	Comp. het.	(brother with p.A11G/ c.C32G, p.N412K/ c.T1236T	none	(43)	R_003
c.C32G	c.T1236T	p.A11G	p.N412K	Comp. het.	(brother with p.A11G/ c.C32G, p.N412K/ c.T1236T	none	(43)	R_004
c.T57G	c.1904delA	p.L19W	p.K635fs*10X	Comp. het.		none	(44)	R_005
c.597_600delTCAG	c.597_600delTCAG	p.Q200Kfs*201	p.Q200Kfs*201	Homo.		none	(45)	R_006
c.597_600delTCAG	c.597_600delTCAG	p.Q200Kfs*201	p.Q200Kfs*201	Homo.		none	(45)	R_007
c.597_600delTCAG	c.597_600delTCAG	p.Q200Kfs*201	p.Q200Kfs*201	Homo.		none	(45)	R_008
c.613delT	c.1904delA	p.S205Lfs*29X	p.K635fs*10X	Comp. het.		generalised erythema and dry cracked skin	(46, 47)	R_009
c.613delT	c.C845A	p.S205Lfs*29X	p.H282L	Comp. het.	balanced translocation t(1;19)(q21;p13))	hepatomegaly, skin scaly, dry, pale, hair was dry, brittle and scarce	(48)	R_010
c.613delT	c.C845A	p.S205Lfs*29X	p.H282L	Comp. het.	balanced translocation t(1;19)(q21;p13))	NA	(48)	R_011
c.613delT	c.C2440T	p.S205Lfs*29X	p.R814X	Comp. het.		none	(46, 49, 50)	R_012
c.A745G	c.1270_1274delAAAGA	p.M249V	p.K424Rfs*20X	Comp. het.		none	(51)	R_013
c.A745G	c.1271_1275delAAAGA	p.M249V	p.K424Rfs*20X	Comp. het.		jaundice, sclerosing cholangitis, hepatosplenomegaly	(43)	R_014
c.A745G	c.1271_1275delAAAGA	p.M249V	p.K424Rfs*20X	Comp. het.		jaundice, sclerosing cholangitis, hepatosplenomegaly	(43)	R_015
c.G827A	c.233_236delAGAG	p.G276D	p.R78Wfs*15X	Comp. het.		disseminated erythematous maculopapules after Rubella vaccine, hepatosplenomegaly.	(52)	R_016
c.G833A	c.G833A	p.R278H	p.R278H	Homo.		NA	(53)	R_017
c.G833A	c.G833A	p.R278H	p.R278H	Homo.		hypopigmentation, bronchiectasis	(44)	R_018
c.G833A	c.G833A	p.R278H	p.R278H	Homo.		hypopigmentation	(44)	R_019
c.G833A	c.G833A	p.R278H	p.R278H	Homo.	for all 3 mutations + p.A3V + p.T9I/ c.C8T + c.C26T	none	(54-57)	R_020
c.G833A	c.G833A	p.R278H	p.R278H	Homo.		none	(54, 58, 59)	R_021
c.G833A	c.1271_1275delAAAGA	p.R278H	p.K424fs*20X	Comp. het.		NA	(60)	R_022
c.G833A	c.1271_1275delAAAGA	p.R278H	p.K424fs*20X	Comp. het.		NA	(53)	R_023

c.G833A	c.1271_1275del	p.R278H	p.K424Rfs*21X	Comp. het.		NA	(10)	R_024
c.G833T	c.G833T	p.R278L	p.R278L	Homo.		none	(35, 61)	R_025
c.G833T	c.G833T	p.R278L	p.R278L	Homo.		none	(35)	R_026
c.G833T	c.935delC	p.R278L	p.P313Hfs*19	Homo.		AIHA	(35, 61)	R_027
c.G833T	c.1142_1143delCT	p.R278L	p.L382Efs*4	Comp. het.	c.C26T/ p.T9I	AIHA	(35, 61)	R_028
c.G833T	c.1144_1145delCT	p.R278L	p.L382Efs*5	Comp. het.		gastrointestinal ulcers	(62)	R_029
c.G833T	c.1271_1275delAAAGA	p.R278L	p.K424Rfs*20X	Comp. het.		vitiligo	(62)	R_030
c.G833T	c.1271_1275delAAAGA	p.R278L	p.K424Rfs*20X	Comp. het.		erythroderma	(62)	R_031
c.G833T	c.1271_1275delAAAGA	p.R278L	p.K424Rfs*20X	Comp. het.		eczema, generalized lymphadenopathy	(62)	R_032
c.G833T	c.1271_1275delAAAGA	p.R278L	p.K424Rfs*20X	Comp. het.		none	(62)	R_033
c.G833T	c.1271_1275delAAAGA	p.R278L	p.K424Rfs*20X	Comp. het.		none	(62)	R_034
c.G833T	c.1271_1275delAAAGA	p.R278L	p.K424Rfs*20X	Comp. het.		none	(35, 61)	R_035
c.G833T	c.1271_1275delAAAGA	p.R278L	p.K424Rfs*20X	Comp. het.		colitis	(35, 61)	R_036
c.G833T	c.1271_1275delAAAGA	p.R278L	p.K424Rfs*20X	Comp. het.		AIHA, purpura	(35)	R_037
c.G833T	c.1271_1275delAAAGA	p.R278L	p.K424Rfs*20X	Comp. het.		none	(35)	R_038
c.G833T	c.1271_1275delAAAGA	p.R278L	p.K424Rfs*20X	Comp. het.		AIHA	(35)	R_039
c.G833T	c.1271_1275delAAAGA	p.R278L	p.K424Rfs*20X	Comp. het.		anti-human globulin test, anti-thrombocytes antibodies, anti-HLA antibodies	(63)	R_040
c.G833T	c.1277_1278delAA	p.R278L	p.E426Gfs*19	Comp. het.		none	(62)	R_041
c.G833T	c.G2113T	p.R278L	p.E705X	Comp. het.		none	(35, 61)	R_042
c.G833T	c.2134_2135delTA	p.R278L	p.I712Afs*5	Comp. het.		AIHA	(35, 61)	R_043
c.G833T	c.C2710T	p.R278L	p.Q904X	Comp. het.	p.S12T / c.T34A	none	(35)	R_044
c.G833T	loss exon2 (189-4043)	p.R278L	none	Comp. het.		none	(35)	R_045
c.G833C	NA	p.R278P	p.E582Dfs	Comp. het.		none	(64)	R_046
c.A840G	c.1271_1275delAAAGA	p.Q280R	p.K424Rfs*20X	Comp. het.	no AV3, T9I	none	(34, 57)	R_047
c.A840G	c.1271_1275delAAAGA	p.Q280R	p.K424Rfs*20X	Comp. het.	no AV3, T9I	none	(34, 57)	R_048
c.A845T	c.1544_1548delAAAGA	p.H282L	p.K424Rfs*19X	Comp. het.		veno-occlusiv disease	(33, 57)	R_049
c.A845T	c.1544_1548delAAAGA	p.H282L	p.K424Rfs*19X	Comp. het.		autoimmune cytopenia	(33, 57)	R_050
c.C845T	c.1746_1750delAAGAT	p.H282L	p.R581fsX	Comp. het.	c.C26T/ p.T9I	Omenn syndrome (scaly eryhroderma), hepatosplenomegaly, lymphadenopathy	(57, 65)	R_051
c.C847G	c.C847G	p.K283E	p.K283E	Homo.		NA	(66)	R_052

c.A847A	c.1271_1275delAAAGA	p.K283E	p.K424Rfs*20X	Comp. het.		NA	(67)	R_053
c.A847A	c.1271_1275delAAAGA	p.K283E	p.K424Rfs*20X	Comp. het.		none	(67)	R_054
c.A875G	c.1307_1311del	p.Q229R	p.K436Rfs*20	Comp. het.		NA	(10)	R_055
c.G907A	c.1904delA	p.P231T	p.A562fs21X	Comp. het.		None	(68)	R_056
c.T980G	c.2585_5886del	p.I327S	p.H826Rfs*6	Comp. het.		AIHA	(35)	R_057
c.G1102T	c.G1102T	p.D368Y	p.D368Y	Homo.		Eczema	(69)	R_058
c.A1103T	c.G1341T	p.D368V	p.W447C	Comp. het.		bronchiectasis, villous atrophy, liver lesions, granulomatous dermatitis (after Rubella vaccination, nodular, superficial and deep dermal lymphohistiocytic infiltrate with scattered lymphohistiocytic cells)	(70)	R_059
c.G1237T	c.G1341	p.E413*	p.W447C	Comp. het.		epithelioid cell granuloma (absence of infection)	(57, 71)	R_060
c.1245_1250dupGATGC	c.C2440T	p.L418Mfs*3	p.R814X	Comp. het.		none	(47)	R_061
c.1271_1274delAAAG	c.C2440T	p.K424Rfs*20X	p.R814X	Comp. het.		NA	(10)	R_062
c.1271_1275delAAAGA	c.C2440T	p.K424Rfs*20X	p.R814X	Comp. het.		psoriasis	(47)	R_063
c.1271_1275delAAAGA	c.C2440T	p.K424Rfs*20X	p.R814X	Comp. het.		none	(47)	R_064
c.1271_1275delAAAGA	c.C2440T	p.K424Rfs*20X	p.R814X	Comp. het.		none	(47)	R_065
c.1271_1275delAAAGA	c.C2440T	p.K424Rfs*20X	p.R814X	Comp. het.		hypopigmentation	(47)	R_066
c.1271_1275delAAAGA	c.C2440T	p.K424Rfs*20X	p.R814X	Comp. het.		none	(47)	R_067
c.1271_1275delAAAGA	c.C2440T	p.K424Rfs*20X	p.R814X	Comp. het.		none	(47)	R_068
c.1271_1275delAAAGA	c.C2440T	p.K424Rfs*20X	p.R814X	Comp. het.		none	(67)	R_069
c.1271_1275delAAAGA	c.C2440T	p.K424Rfs*20X	p.R814X	Comp. het.		cutaneous abnormalities	(66)	R_070
c.A1296T	c.C1672T	p.K432N	p. Q558X	Comp. het.		none	(35)	R_071
c.1297_1299delCAA	c.1297-1299delCAA	p.Q433del	p.Q433del	Homo.		none	(57, 72)	R_072
c.T1312c	c.T1312c	p.Y438H	p.Y438H	Homo.	LRIG2 mutations (homo)	nail dystrophy, sparse and thin hair	(73)	R_073
c.A1345C	c.C2440T	p.K449Q	p.R814X	Comp. het.		none	(32)	R_074
c.A1345C	c.C2440T	p.K449Q	p.R814X	Comp. het.		none	(32)	R_075
c.A1345C	c.C2440T	p.K449Q	p.R814X	Comp. het.		none	(32)	R_076
c.A1345C	c.C2440T	p.K449Q	p.R814X	Comp. het.		NA	(53)	R_077
c.G1406A	c.C2440T	p. G469E	p.R814X	Comp. het.		psoriasiform erythrodermic squamous skin patches	(55, 56, 74)	R_078
c.G1406A	c.C2440T	p. G469E	p.R814X	Comp. het.		none	(75)	R_079

c.1512_1513delTC	c.C2440T	p.R505Cfs*12X	p.R814X	Comp. het.		none	(47)	R_080
c.1751_1755delTAAGA	c.C2440T	p.I584Rfs*2X	p.R814X	Comp. het.		none	(76)	R_081
c.1762delAAG	c.1762delAAG	p.K588del	p.K588del	Homo.		none	(77)	R_082
c.1762delAAG	c.1762delAAG	p.K588del	p.K588del	Homo.		none	(77)	R_083
c.C1738T	c.C2440T	p.R580X	p.R814X	Comp. het.		hypothyroidism, hypogonadism, diabetes, chronic cutaneous affection, photosensitivity, telangiectasia	(55)	R_084
c.C1738T	c.C2440T	p.R580X	p.R814X	Comp. het.		hypothyroidism, amenorrhea, photosensitivity, psoriasis	(55)	R_085
c.1904delA	c.C2440T	p.K635fs*10X	p.R814X	Comp. het.		NA	(66)	R_086
c.1904delA	c.C2440T	p.K635fs*10X	p.R814X	Comp. het.		NA	(66)	R_087
c.C2094T	c.C2440T	p.Y698X	p.R814X	Comp. het.		None	(47)	R_088
c.C2094T	c.C2440T	p.Y698X	p.R814X	Comp. het.	Xp22.31p22.32 duplication	none	(78)	R_089
c.2386_2389dupATTG	c.C2440T	p.A797Dfs*3	p.R814X	Comp. het.		cutis marmorata	(47)	R_090
c.C2440T	c.C2440T	p.R814X	p.R814X	Homo.		hypogonadism, asthma, lymphadenopathy, hepatomegaly.	(79)	R_091
c.G2612A	c.G2612A	p.R871H	p.R871H	Homo.		recurrent meningitis (sterile), recurrent genital/oral ulcers, anterior uveitis, intermittent attacks of non-erosive arthritis.	(80)	R_092
NA	NA	NA	NA	NA	AML: 48, XX, +2, der(5)t(5;17)(q11;q11), -7, +8, +11, -17, +20/46, XX	none	(81)	R_093
NA	NA	NA	NA	NA		none	(57)	R_094
NA	NA	NA	NA	NA		autoimmunity, Omenn phenotype	(57)	R_095
NA	NA	NA	NA	NA		none	(57)	R_096
NA	NA	NA	NA	NA		none	(57)	R_097
NA	NA	NA	NA	NA		none	(57)	R_098
NA	NA	NA	NA	NA		none	(57)	R_099
NA	NA	NA	NA	NA		none	(57)	R_100
NA	NA	NA	NA	NA		none	(57)	R_101
NA	NA	NA	NA	NA		none	(57)	R_102
NA	NA	NA	NA	NA		none	(57)	R_103

NA	NA	NA	NA	NA		none	(57)	R_104
NA	NA	NA	NA	NA		none	(57)	R_105
NA	NA	NA	NA	NA		none	(57)	R_106
NA	NA	NA	NA	NA		autoimmunity	(57)	R_107
NA	NA	NA	NA	NA		none	(57)	R_108
NA	NA	NA	NA	NA		none	(57)	R_109
NA	NA	NA	NA	NA		none	(57)	R_110
NA	NA	NA	NA	NA		none	(57)	R_111
NA	NA	NA	NA	NA		none	(57)	R_112
NA	NA	NA	NA	NA		none	(57)	R_113
NA	NA	NA	NA	NA		none	(57)	R_114
NA	NA	NA	NA	NA		none	(57)	R_115
NA	NA	NA	NA	NA		none	(57)	R_116
NA	NA	NA	NA	NA		none	(57)	R_117
NA	NA	NA	NA	NA		NA	(57)	R_118
NA	NA	NA	NA	NA		NA	(57)	R_119
NA	NA	NA	NA	NA		NA	(57, 82)	R_120

706

707

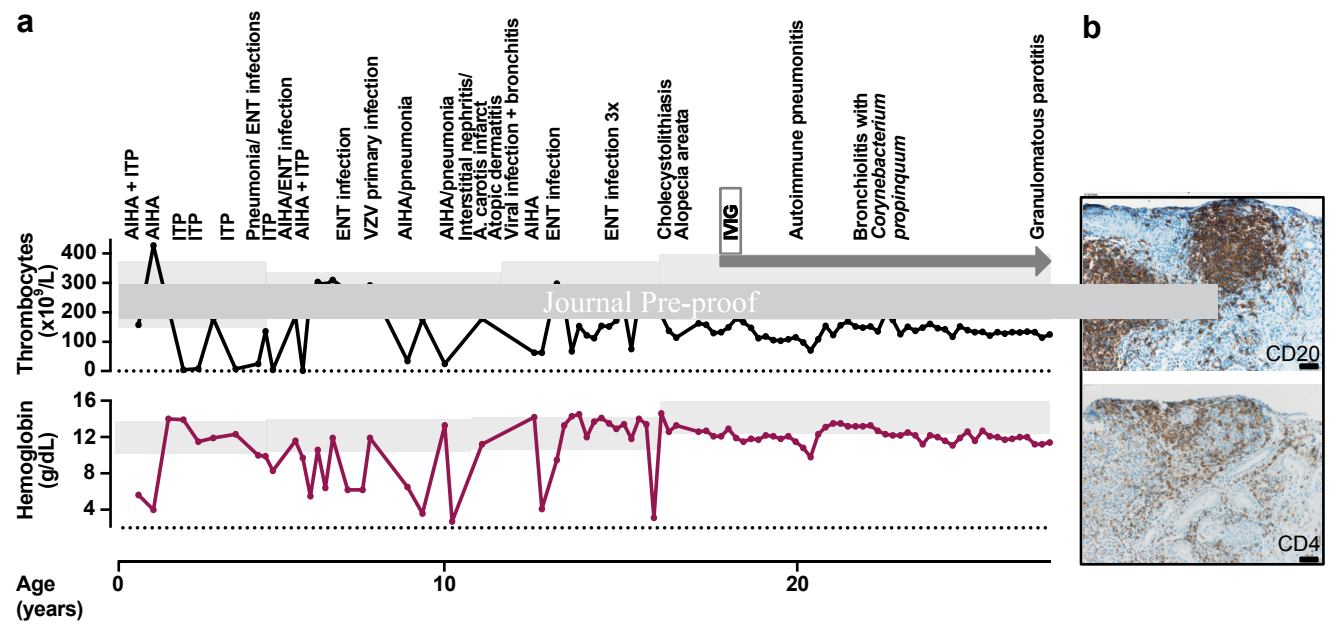

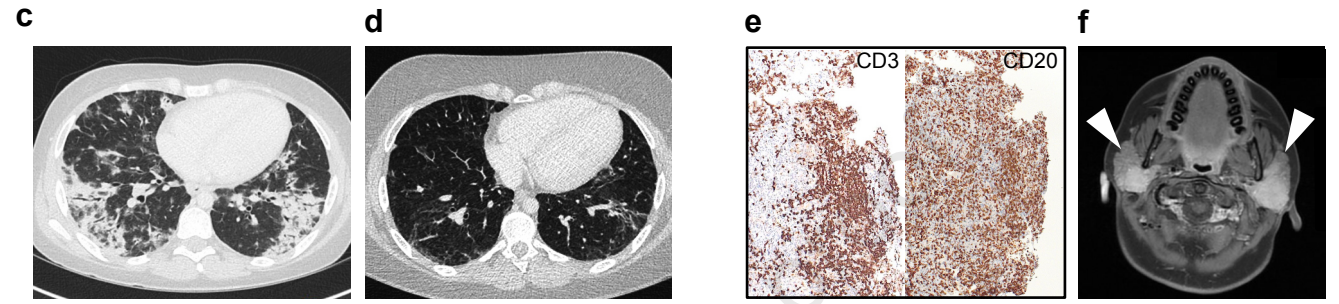

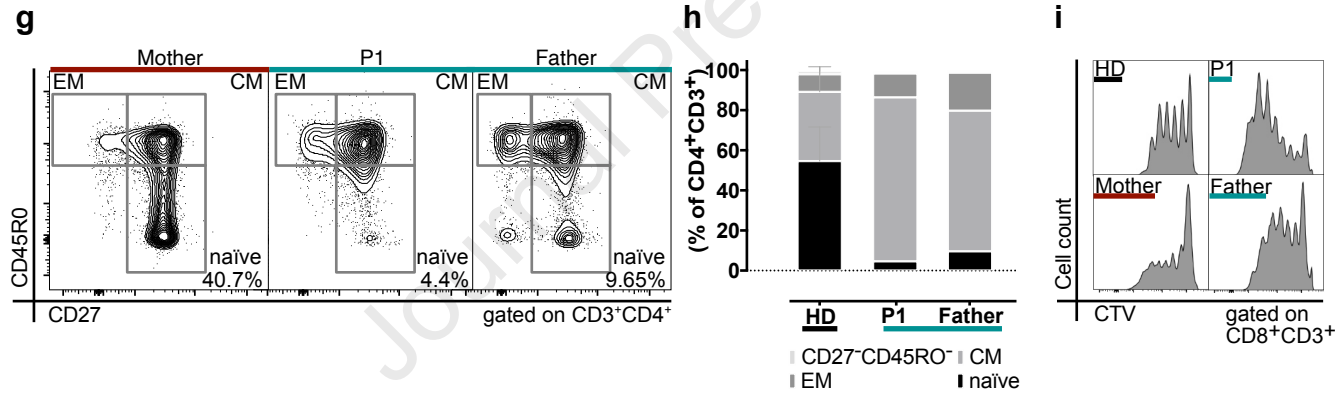

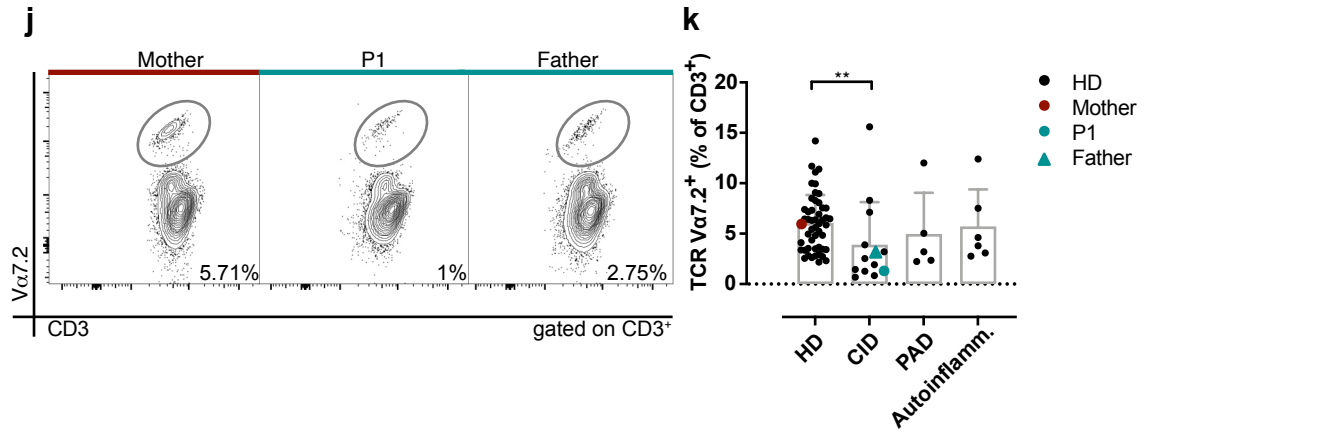

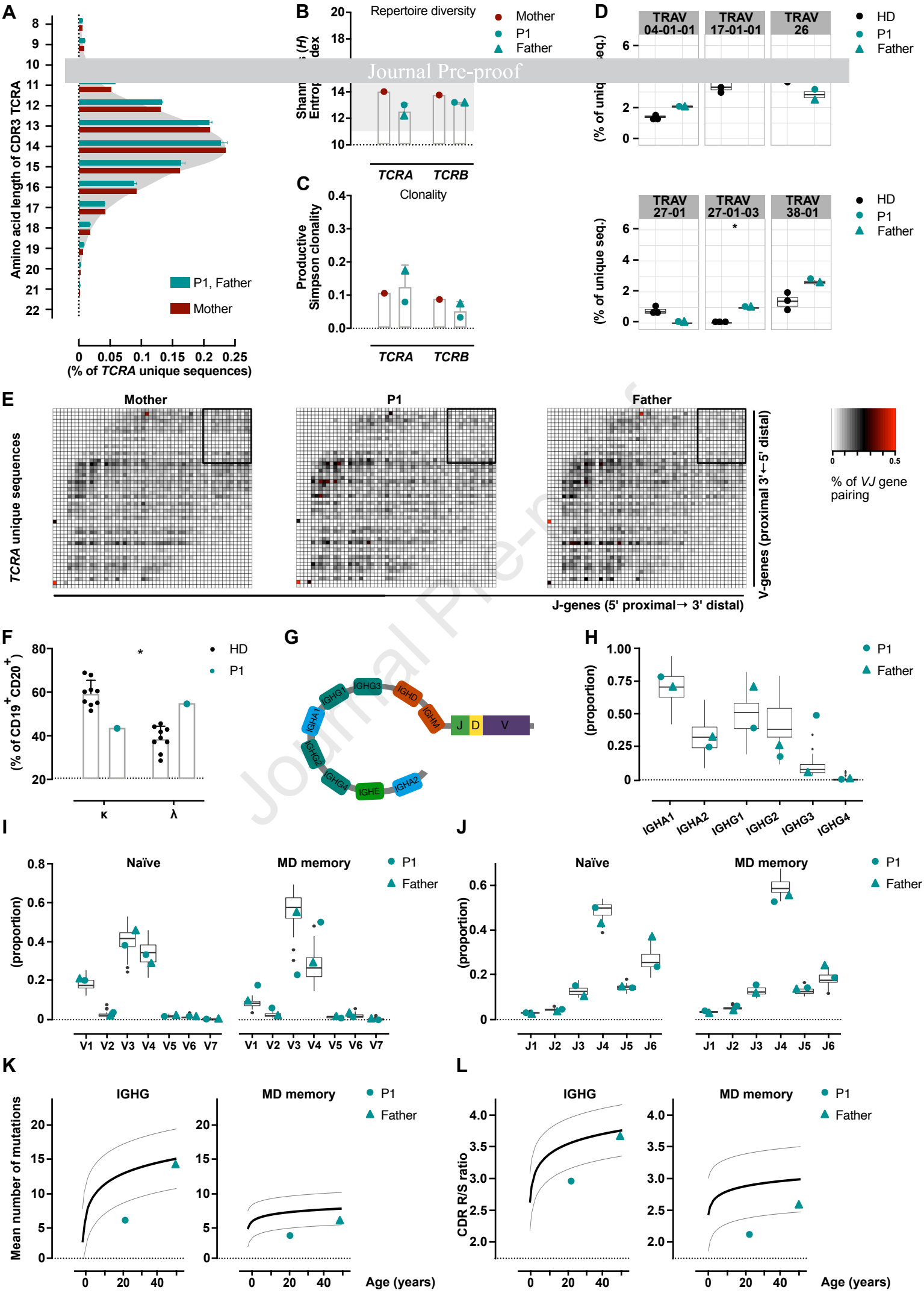

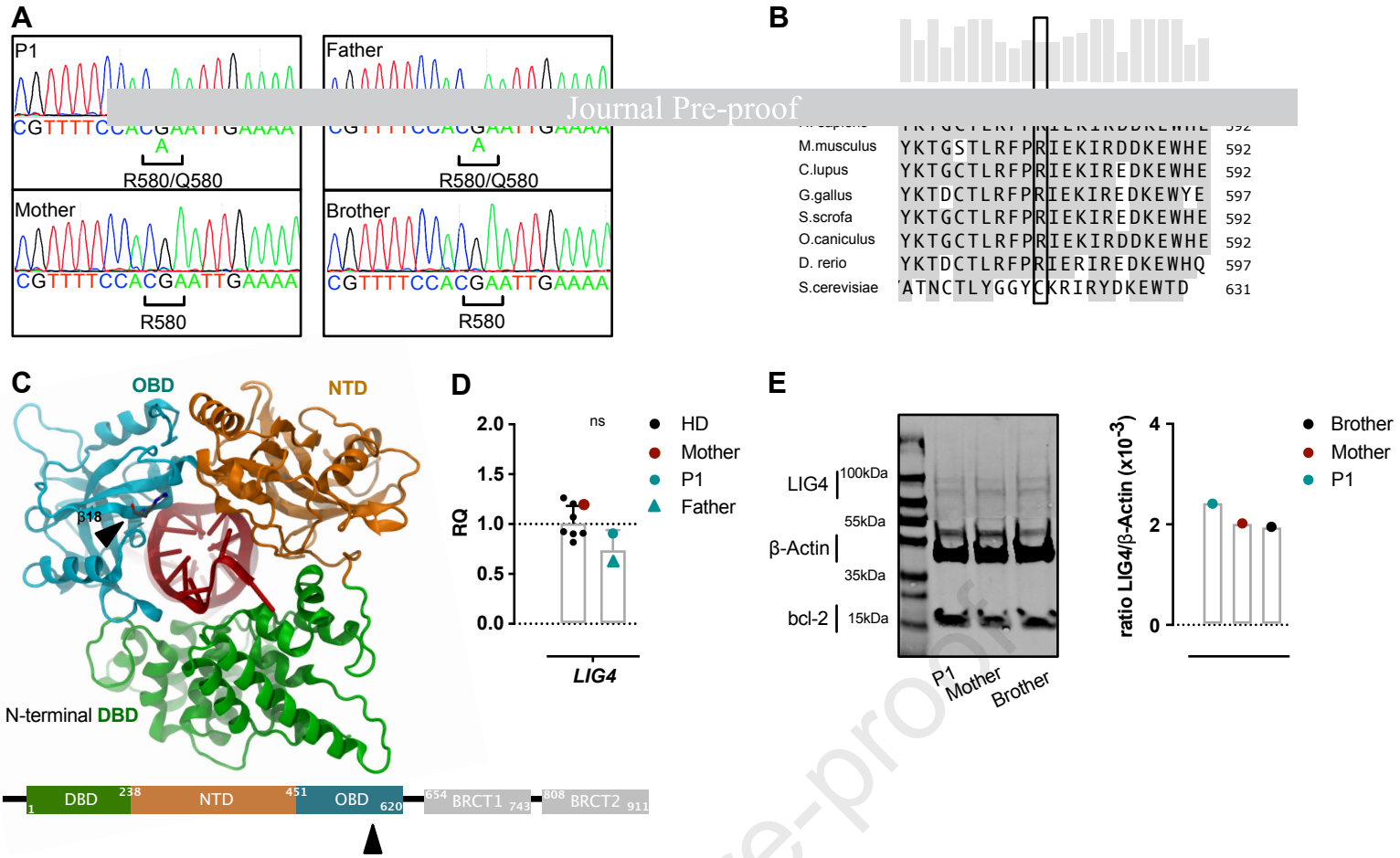

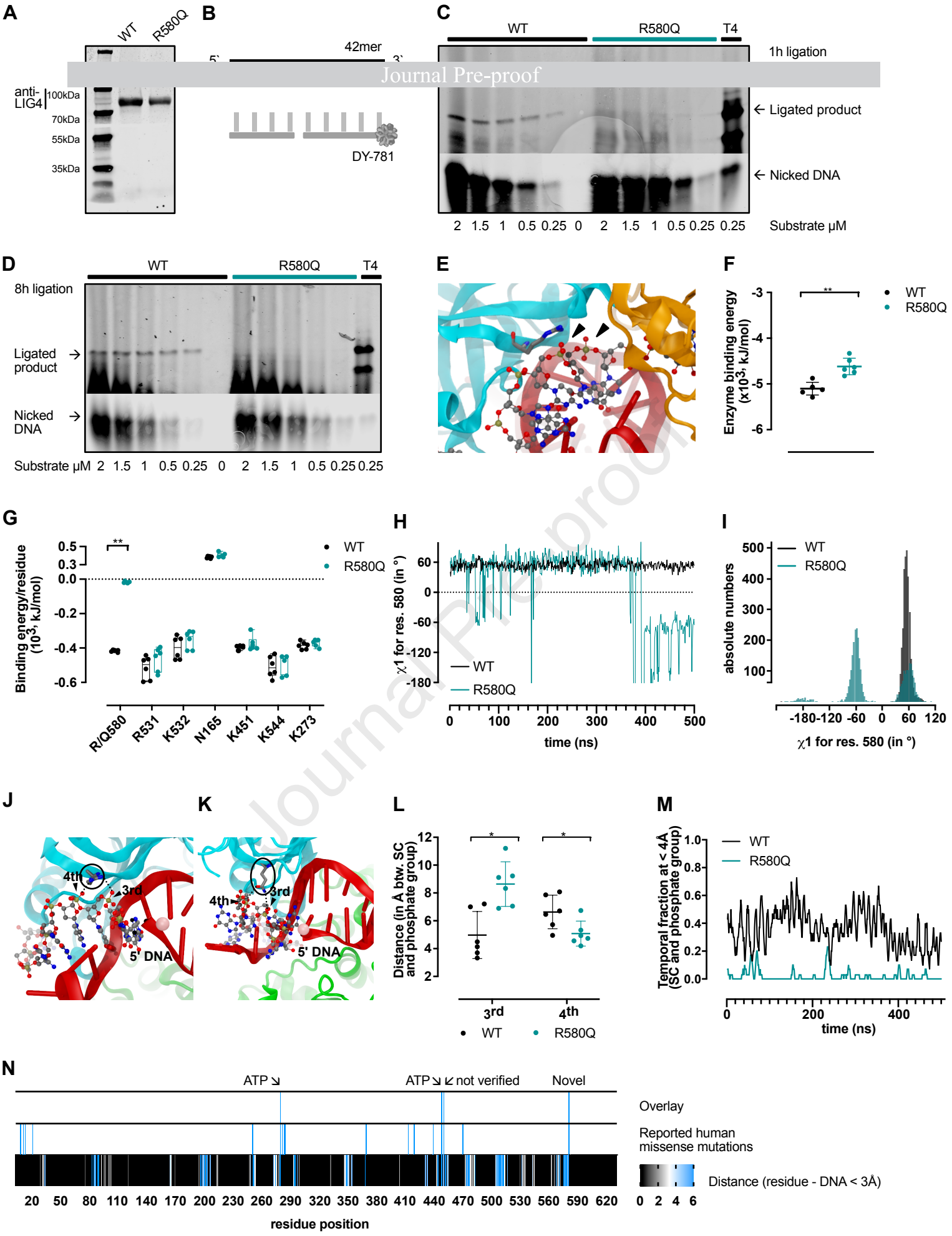

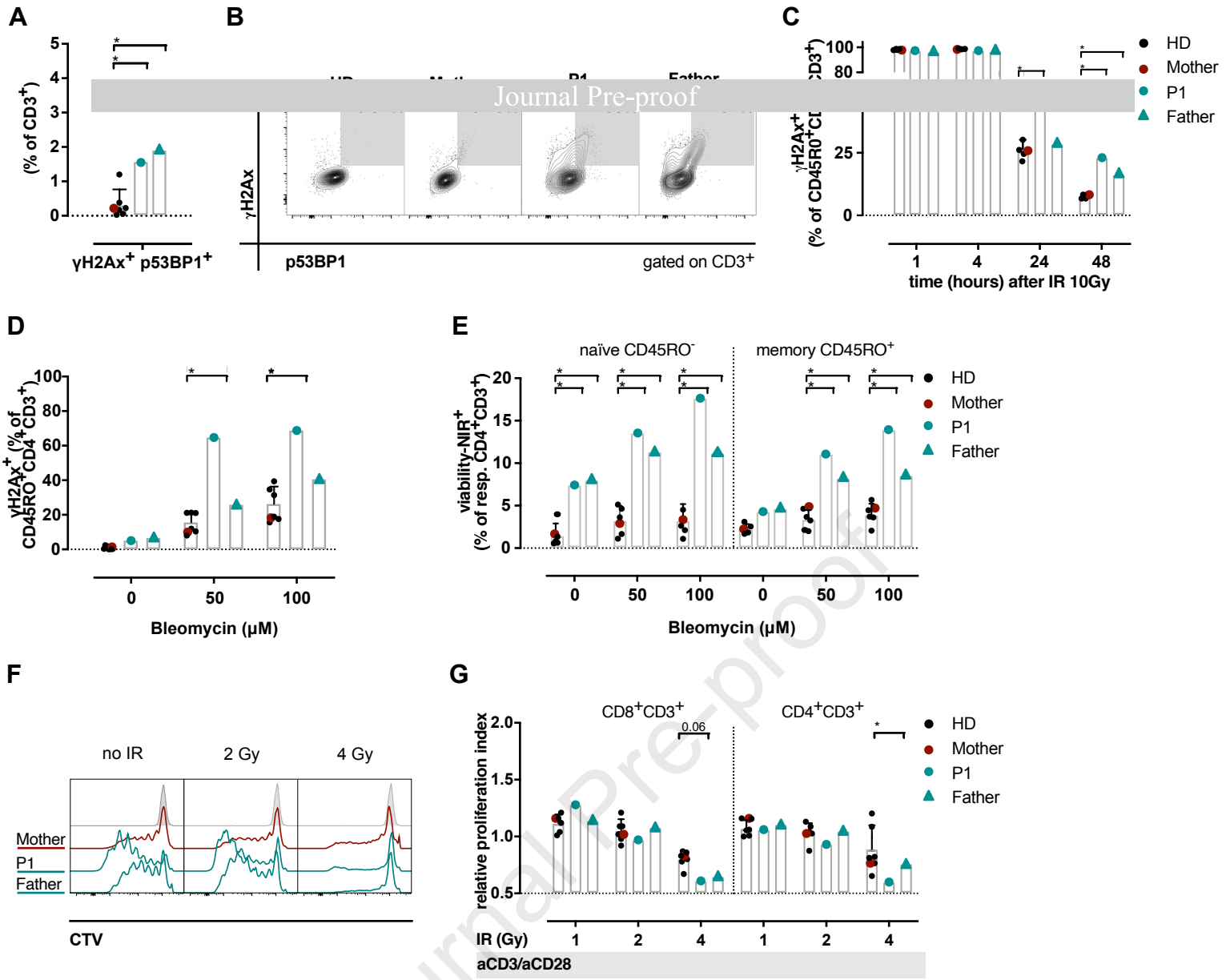

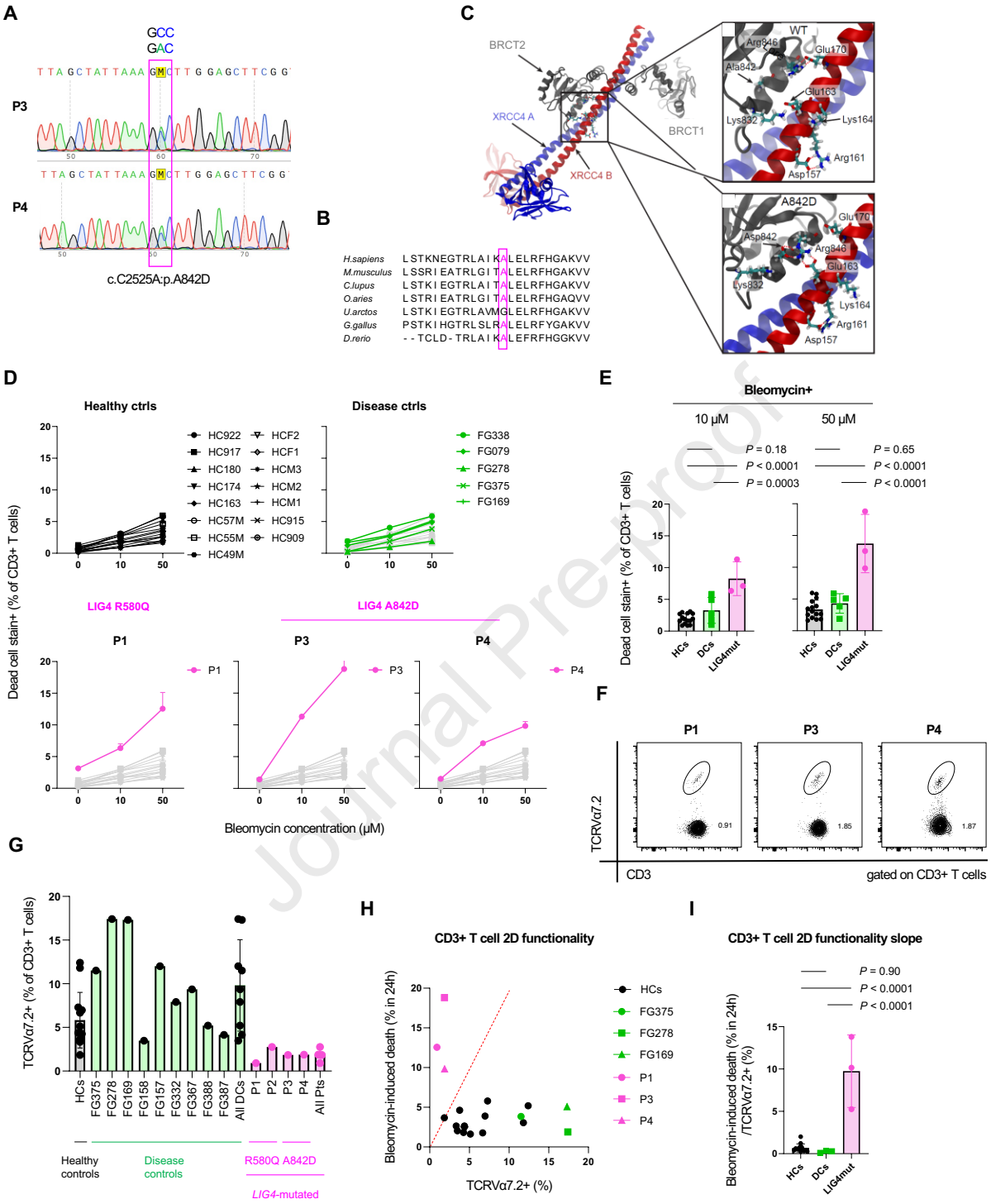
A
GCC
GAC
P3
P4
c.C2525A:p.A842D
B
H.sapiens
M.musculus
C.lupus
O.aries
U.arctos
G.gallus
D.rerio
C
BRCT2
XRCC4 A
XRCC4 B
BRCT1
WT
A842D
D
Healthy ctrls
Disease ctrls
HC922
HC917
HC180
HC174
HC163
HC57M
HC55M
HC49M
HCF2
HCF1
HCM3
HCM2
HCM1
HC915
HC909
FG338
FG079
FG278
FG375
FG169
LIG4 R580Q
LIG4 A842D
P1
P3
P4
Dead cell stain+ (% of CD3+ T cells)
Bleomycin concentration (μM)
E
Bleomycin+
10 μM
50 μM
P = 0.18
P < 0.0001
P = 0.0003
P = 0.65
P < 0.0001
P < 0.0001
HCs
DCs
LIG4mut
F
TCRVα7.2
CD3
gated on CD3+ T cells
0.91
1.85
1.87
G
TCRVα7.2+ (% of CD3+ T cells)
All DCs
All Pts
Healthy controls
Disease controls
R580Q A842D
LIG4-mutated
H
CD3+ T cell 2D functionality
Bleomycin-induced death (% in 24h)
TCRVα7.2+ (%)
I
CD3+ T cell 2D functionality slope
P = 0.90
P < 0.0001
P < 0.0001
Bleomycin-induced death (% in 24h) /TCRVα7.2+ (%)